KUNSTSTOFF TECHNIK LEOBEN

CHEMIE DER KUNSTSTOFFE

Master Thesis

Coupling of functionalised PTHF to amine-modified silica particles via aza-Michael reaction

Julia Winter

supervised by
Univ. Prof. Dr. Wolfgang Kern

in cooperation with

getzner
engineering a quiet future

Leoben, November 2016

Abstract

The aim of this master thesis is to lay the chemical foundations for the development of materials based on silica particles and the polyetherol polytetrahydrofurane (PTHF).

Therefore, three steps were taken: a) an end-group modification of PTHF, b) the characterisation of silica particles and c) investigations on reaction conditions for the coupling of silica particles to the functionalised polyols.

The esterification of PTHF with organic acid was conducted successfully at high yields. The purification procedure described in literature was adapted and the products were characterised via FTIR, NMR, TGA and wet-chemical methods. The functionality of commercially available surface-modified silica particles was determined with TGA, titration and elemental analysis, which led to equivalent results. After examining numerous catalyst systems, partial conversion was observed for functionalised polyetherol and amines under aqueous conditions and microwave-induced heating. Experiments on coupling of silica particles to the functionalised polyols showed promising results.

Kurzfassung

Das Ziel dieser Masterarbeit ist es, die chemischen Grundlagen für die Entwicklung eines Materials aus Silikapartikeln und dem Polyetherol Polytetrahydrofuran (PTHF) zu legen.

Dazu sind drei Schritte notwendig: a) die Endgruppen des PTHFs zu modifizieren, b) die Silikapartikel zu charakterisieren und c) geeignete Reaktionsbedingungen für die Kopplung der Silikapartikel an die funktionalisierten Polyetherole zu finden.

Die Veresterung von PTHF mit organischer Säure wurde erfolgreich mit hohen Umsätzen durchgeführt. Eine neue Reinigungsvorschrift wurde entwickelt und die Produkte mittels FTIR, NMR, TGA und nasschemischer Analyse untersucht. Die Funktionalität der kommerziell verfügbaren Silikapartikel wurde mittels TGA, Titrationen und Elementaranalyse ermittelt, was äquivalente Ergebnisse lieferte. Nach der Untersuchung verschiedener Katalysesysteme wurde eine teilweise Umsetzung des funktionalisierten Polyetherols mit Aminen in wässrigem Medium bei Energiezufuhr mittels Mikrowelle beobachtet. Erste Experimente zur Kopplung der Silikapartikel mit den funktionalisierten Polyolen lieferten vielversprechende Ergebnisse.

Affidavit

I declare in lieu of oath, that I wrote this thesis and performed the associated research myself, using only literature cited in this volume.

Eidesstattliche Erklärung

Ich erkläre an Eides statt, dass ich diese Arbeit selbstständig verfasst, andere als die angegebenen Quellen und Hilfsmittel nicht benutzt und mich auch sonst keiner unerlaubten Hilfsmittel bedient habe.

Ort, Datum	Unterschrift

Acknowledgement

Scientific work and writing a thesis brings about the realisation that even at the end of my studies, it was just a sip out of the ocean of knowledge I have been able to acquire. Although this work tested skills such as patience and endurance, I consider it as one of the best parts of my studies. This is due to the great support and the amazing people I was allowed to work with! I was given independence, but at the same time I never felt left alone.

First of all, I want to thank my advisers: Wolfgang Ziegler to whose PhD thesis my work is linked and assistant professor Gisbert Rieß. In my eyes it is a strong sign of confidence to share such a crucial and interesting part of this project with me. Thank you for the vivid discussions, for cheering me up in moments of desperation, for your patience, guidance and ideas, but most of all for your dear friendship!

I would like to express my gratitude towards professor Wolfgang Kern and all my colleagues of the Department of Chemistry of Polymeric Materials at Montanuniversität Leoben, for creating a productive and welcoming atmosphere, it is a pleasure to work in. Especially, I would like to point out Baris Kaynak, who taught me the practical aspects of synthetic chemistry. Another great chemist I want to thank is Mathis Reinfelds, his hint helped me to solve one of the most difficult riddles that occurred in the work.

I am grateful towards our company partner Getzner Werkstoffe GmbH. The months spent in Vorarlberg at their plant brought about that coming back to Bürs feels like coming home. This is related to the wonderful working environment. Special thanks go to Sven Müller, Stefan Kopeinig and Martin Dietrich: I will never forget the discussions, the ideas you contributed to this work and the hours passed in the laboratory together!

I want to thank the Austrian Research Promotion Agency FFG for their financial support, which made the project possible. I am grateful towards the Institute for Inorganic Chemistry of the Technical University of Graz (TU Graz) for performing dynamic light scattering measurements. Furthermore, I want to thank the microanalytical laboratory of the Faculty for Chemistry of the University of Vienna for performing elemental analysis.

Finally and most of all, I want to take this opportunity to thank my family for their support, motivation, interest and love I have experienced all my life.

Contents

Chapter 1

Introduction

Bionics, the attempt to imitate biological materials, is a common approach in nanotechnology. In this project, a similar yet unusual way is chosen: trying to imitate a class of synthetic materials. The general aim is to develop nanocomposites with similar morphological structures as polyurethane elastomers (PUR).

Polyurethanes are formed by polyaddition of diisocyanates to polyethers or polyesters with alcohol end-groups (polyols). Their applications are wide – modern life can hardly be imagined without these materials, which date back to Otto Bayer in 1937. Their properties can be tuned easily upon wide ranges: synthetic leather, hard and soft foams, resistant coatings, sealants, textiles (Elastan®) and adhesives are only a few examples. They are cheap and easy to process, furthermore, tailored material behaviour can be reached by adaptation of the chemical components. For some applications, such as vibration absorbance, the key to success lies on a smaller level: in its nanostructure [1].

The most significant morphological characteristic of polyurethane elastomers is the phase separation between the hard and soft segments. The flexible polyol soft segments exhibit entropy-elastic behaviour, as their glass transition temperature is below room temperature (-30 to -70 °C). The embedded hard segments are dominated by rigid aromatic structures of the diisocyanates and hydrogen bonding of the urethane groups. Their glass transition lies above operational temperature. Therefore, they are not only reinforcing the polymer, but also lead to physical cross-linking [1].

By transmission electron microscopy studies in the 1970s, the size of the hard segments was found to range between 3 and 10 nm [2] or 20 and 30 nm [3]. This makes polyurethanes nano-structured materials.

Despite their undoubted advantages as materials, classical production of polyurethanes is considered more and more critical in therms of toxicology and safety. This tendency is noticed in legal regulations: In 2015, the Environmental Protection Agency (EPA) of the United States released

a Significant New Use Rule for toluidene diisocyanate (TDI), one of the most common diisocyanates. It implies the duty to report the use of those substances in new products with the aim to evaluate and regulate it [4].

The extensive work on the health hazard of diisocyanates was reviewed by Allport, Gilbert, and Outterside [5]. They point out that hypersensitivity of staff working with isocyanates has been reported. Diisocyanates especially jeopardize the respiratory tract, notably by causing asthma [6].

In view of this, the aim of this thesis is to contribute to the development of a material, which reaches the properties of polyurethanes without the use of isocyanates: isocyanate-free polyurethanes have been the focus of numerous studies. Latest work was concisely reviewed by Rokicki, Parzuchowski, and Mazurek [7]. Herein, isocyanate-free synthesis routes are classified in three main approaches: polycondensation, ring-opening polymerisation and step-growth polyaddition. The most auspicious results are derived from the last category by using bis-functional reactands containing amine and cyclic carbonate endgroups [8]. Coating systems, rigid and soft foams based on this reaction are already commercially available (Green Polyurethane™) [9].

Despite the promising findings to establish isocyanate-free polyurethanes via pure organic chemistry, we chose to study whether those structures are also realisable through nanocomposites. In this area, only little work has yet been done: Birukov et al. invented a sol-gel chemical process to obtain interpenetrating polymer networks from compositions with amine, epoxy and cyclic carbonate functional units. One of these components includes alkoxysilane structures that undergo hydrolytic condensation [10, 11]. Türünç et al. followed a different approach: they synthesized cyclic carbonate functionalised silica nanoparticles which reacted with diamines to form network structures [12]. Increased thermal stability as well as improved abrasion resistance for coatings were observed. The findings of Gaharwar et al. for silicate reinforced polyethylene glycol (PEG), which forms transparent, elastomeric and tough hydrogels [13], reassured us to pursue our aim of research. Polyurethane-like elastomer structures should be achieved with the following characteristics:

- The soft segment is built up from PTHF and therefore comparable to known polyurethane systems.
- The hard segment is replaced by commercially available inorganic nanoparticles. Due to inorganic hard segments, a change in mechanical performance and decreasing temperature dependence of the material is expected.
- A stable and covalent connection between the segments needs to be ensured.

This concept is illustrated in figure 1.1.

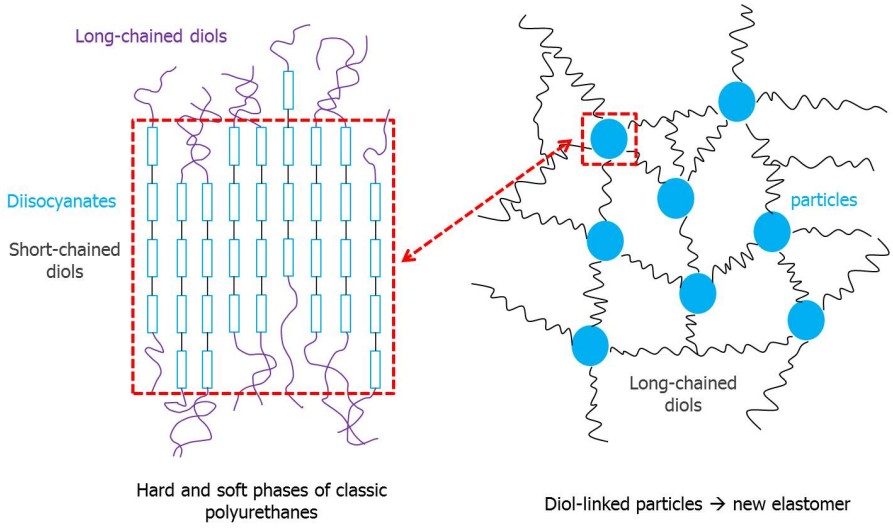

Figure 1.1: Scheme of the structure of the desired nanocomposites in comparison to polyurethane elastomers; the red boxes indicate structures of equal size

The aim of this thesis is to effectuate covalent coupling between particles and polyols and hence lay the foundation for further development. Although large efforts have already been taken in the field of nanoparticle modification, only a few species of modified particles are commercially available. Therefore, amine-modified silica nanoparticles were chosen. Polyols are a moderately reactive chemical substance – no purchasable particles were found that could directly react with them. Thus, this necessitated the modification of polyols. Amongst a variety of groups, which might react with amines, such as epoxy, carboxylic acids and isocyanates, acrylates were chosen for two reasons: Firstly, a simple synthesis route to obtain acrylated PTHF is described in literature. Secondly, besides reactions with amines via Michael reaction, acrylate groups can react with each other upon photochemical or radical stimulation. This renders a two-step curing process possible. Other publications found on acrylated polyols discuss these curing methods [14, 15, 16].

Consequently, three major tasks have been defined. They are necessary pre-steps for the development of the nanocomposite and structure the experimental part of this thesis:

1. Acrylation of PTHF of different molar mass
2. Characterisation of purchased amine-modified silica nanoparticles
3. Study on the Michael reaction between acrylated PTHF and amines as preliminary work for the coupling of nanoparticles

In step 1, the synthesis and purification of acrylated PTHF of molar masses M between 250 and 2900 g/mol were conducted based on literature. In this step, the procedure for purification for scaled-up batches of 800 g PTHF was improved. The products were characterised via Fourier transform infrared spectroscopy (FTIR), nuclear magnetic resonance spectroscopy (NMR), thermogravimetric analysis (TGA), wet-chemical analysis and pyrolysis gas chromatography-mass spectroscopy (pyGCMS). Degrees of conversion of 80-90 % were reached.

Step 2 was necessary, as the data provided by the supplier of nanoparticles were not sufficient for stoichiometric calculations and mixtures. The nanoparticles were characterised in terms of size (via dynamic light scattering (DLS)) and modification (via FTIR, thermogravimetric analysis (TGA) titrations and elemental analysis). The results of modified and non-modified particles were compared. The degree of modification was determined to be approximately 2-2.5 mmol amines per gram nanoparticles. The nanoparticles specified to have diameters of 10-20 nm were exhibiting hydrodynamic radii of 8-110 nm.

Step 3 formed the most innovative part of this work. The aza-Michael reaction was largely studied for low-molecular substances [17], however, polymeric materials with acrylate end-groups have not been in the focus as they are not easily available.

To examine reaction conditions and catalysts, preliminary experiments were necessary. Finally, microwave-induced reaction with water as catalyst or an aqueous boric acid solution gave promising results for a reaction of acrylated PTHF and decylamine. Due to the poor miscibility of reactants and water, the reaction mixtures were inhomogeneous and therefore difficult to analyse. To overcome this problem, another series was performed in ethanol solution. It was possible to prove that side reactions with the solvent ethanol occurred.

The formation of network structures would have exceeded the range of this thesis and will be the subject of a further study. In final experiments, acrylated PTHF and silica nanoparticles were brought to reaction in ethanol with water as a catalyst. The experiment led to promising results; a decrease of acrylate functionality was observed.

Chapter 2

Theoretical Framework

2.1 Polymer chemistry

2.1.1 Macrodiols

As already mentioned in the introduction, polyurethanes gain their characteristic properties from their two-phased nature consisting of soft and hard segments. Herein, the soft segments are dominated by macromolecular bifunctional alcohols, so-called diols or polyols. Their molar masses range from 500-5000 g/mol, those with 1000-2000 g/mol are the most important. Although any macromolecule with alcohol end-groups could couple with isocyanates to form urethane groups, two main groups of macrodiols are established: polyether- and polyester-based diols. Ester bonds are more polar than ether bonds. Therefore, in combination with urethane groups they lead to better mechanical performance, as well as less phase separation and higher temperature dependence of mechanical properties. Polyester-polyurethane foams are classified as hard foams due to their rigidity. Ester bonds are less resistant to hydrolysis, consequently, polyesterols include important biodegradable polymers such as polycaprolacton.

This project aims to imitate soft foams, therefore a polyetherol was chosen. Poletherols are formed by base-catalysed ring-opening polymerisation of cyclic ethers. The most important representatives of this group are epoxy rings and tetrahydrofurane. Ethylene oxide forms polyethylene glycol (PEG), propylene oxide forms polypropylene oxide (PPO). Tetrahydrofurane is a cyclic ether with 4 carbon atoms. It is the monomer to form polytetrahydrofurane (PTHF), which is also referred to as polytetramethyleneoxide (PTMO). It exhibits strength hardening and a very regular and hence crystallising structure. The number of non-reactive end-groups is usually close to the theoretical maximal value. PTHF-based polyurethanes exhibit the best mechanical performance of all polyether-polyurethanes [1].

2.1.2 Esterification

Esterification is a well-established standard reaction in organic chemistry of an alcohol and a carboxylic acid which forms water and an ester group (RC(=O)OR). This is illustrated in figure 2.1. The reaction is catalysed by acids. It is a equilibrium reaction: to attain high yield, either the educts have to be present in excess or the product needs to be removed. This can be effectuated by using a Dean-Stark receiver.

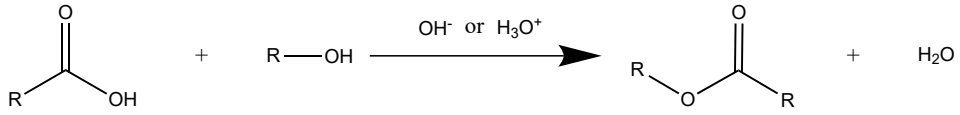

Figure 2.1: Scheme of esterification reactions

Ester bonds are sensitive to alkaline hydrolysis (saponification), which breaks the ester bond. Another important reaction of esters is the reaction with alcohols. During this so-called trans-esterification, the rest groups of alcohol and ester are exchanged. Besides other applications, this reaction is of special importance for the production of polyesters [18, 19].

2.1.3 Michael reaction

The Michael reaction – named after the US-chemist Arthur Michael (1853-1942) – draws great interest in organic synthesis [19]. During this reaction, a nuclecophilic agent (Michael donor) adds to the β-carbon atom of an α,β-unsaturated carbonyl compound (Michael acceptor). According to a narrow definition, the term "Michael reaction" is only valid, if enolates play the role of the nucleophile to form carbon-carbon bonds [19]. However, other sources apply a wider definition, not restricting the range of nucleophiles. To simplify comprehension, prefixes specifying the nucleophile are used in literature: for instance carbon-Michael reaction, aza-Michael reaction or thiol-Michael reaction [20]. The reaction mechanism as an example for a primary amine as nucleophile is shown in figure 2.2.

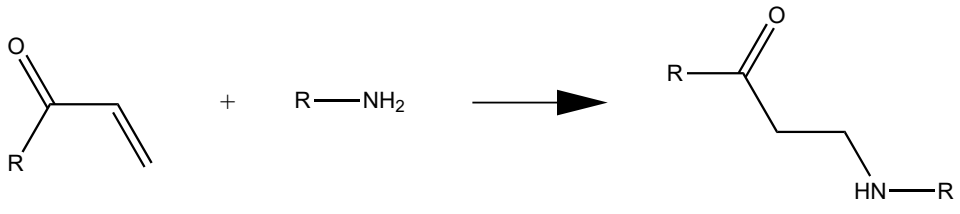

Figure 2.2: Schematic representation of the aza-Michael reaction

In the following, characteristics of the Michael reaction are discussed in detail. A carbonyl compound contains a carbonyl group (C=O); aldehydes,

ketones and carboxylic acid derivates are the most significant examples [19]. The carbonyl group is highly polar: as the electonegative oxygen draws the electrons of the π-bond, it renders the carbon atom easily accessible for nucleophilic attack [18].

According to a widely used nomenclature rule, the carbon atoms of a compound comprising a reactive group are enumerated by Greek letters [21]. This nomenclature bears the following advantage compared to IUPAC rules: the reactivity of carbon atoms close to the specified reactive group can be discussed independently of the structure of the entire molecule. The starting point α is set on the atom neighbouring the reactive group; in case of the Michael acceptor, the carbon atom neighbouring the carbonyl group. Consequently, α,β-unsaturated carbonyl compounds have a double bond between the carbon neighbouring the (C=O) group and the next one. Therefore, the carbon-carbon double bond and the C=O bond form a conjugated structure. It is more stable than a non-conjugated similar compound.

The carbonyl group draws electrons. This polarity is transmitted across the vinyl group by the effect of vinylogy: if groups are connected via vinylene groups, they act as if they were neighbouring each other [22]. Therefore, the electron-drawing effect of the oxygen is transmitted to the β-carbon. This renders the electron density on the α-carbon higher than on the β-carbon. Consequently, the β-carbon is easier accessible for nucleophilic attack, whereas the α-carbon shows H-acid behaviour.

Reactions can occur on each of the double bonds. However, products of the conjugated addition are in general more stable and therefore preferred, due to vinylogy. The mechanism of the Michael reaction is a 1,4-addition followed by the protonation of the α-carbon. The final product of a 1,2-addition would be equivalent.

Besides the carbon-Michael reaction, which displays a possibility to form carbon-carbon bonds, the Michael reaction with amines as Michael donors (aza-Michael reaction) attracts scientific attention [19]. One of the main fields of its application is synthetic chemistry, especially for biologically active compounds. To give an example, it is an elegant route to form β-amino acids [23, 24]. Recent work on the field of aza-Michael reaction was concisely summarised by Rulev [17].

The work on reactants of low molar mass led to the following findings: in general, aromatic amines are less reactive than aliphatic ones and primary amines are less reactive than secondary ones [25]. Various catalysis strategies were investigated; the main focus was on issues of biochemical synthesis, such as enantiomer selectivity. No literature about macromolecular Michael acceptors was found. The following catalysis strategies for aliphatic amines are described in literature. Their efficiency depends on the nucleophilicy of the amine and the electrophilicy of the Michael acceptor.

Absence of any catalyst Michael reactions are known to be catalysed us-

ing catalytical amounts of alkaline [26, 19]. Due to alkalinity of amines, reactions proceed in the absence of a catalyst. This is the case if the Michael donor is highly nucleophilic and the acceptor is highly electrophilic and no steric hindrance occurs.

Acidic catalysis Chaudhuri et al. describe boric acid as a powerful catalyst for aza-Michael reaction [27].

Lewis acids Numberous Lewis acids have been studied, for example metal chlorides: aluminium chloride ($AlCl_3$) [28], titanium chloride ($TiCl_4$) or iron chloride ($FeCl_3$). Especially transition metal salts were described to show high catalytic activity [17]. These substances are sensitive to hydrolysis at the formation of hydrochloric acid (HCl). To improve processing conditions, grafting the catalyst to silica gel was found effective for $AlCl_3$ [28]. Lanthanide salts such as cerium(IV) ammonium nitrate (CAN) play a special role as they can also act as a catalyst in aqueous solutions [29].

Alkaline catalysis Alkaline catalysis is crucial for carbon-Michael reactions, but due to the alkalinity of amines less important. Some special cases where it applies are described in literature [17].

Water as a solvent By the use of water as a solvent, increased reactivity is observed. The mechanism is explained by the activation of the β-carbon atom as well as the amine by hydrogen bonds [17].

Ionic liquids as a solvent Ionic liquids which exhibit many advantages in terms of health and environmental safety were also found to be efficient catalysts and solvents for Michael reactions [17].

2.2 Nanotechnology

2.2.1 Hybrid nanocomposites

Nanomaterials have gained large interest over the last decades as they are believed to contribute massively to scientific and technological questions of our age [30]. This is due to the fact that properties can be reached through nano-scalation, which have not been attainable by conventional materials [31]. A vast number of effects observed in natural and synthetic nanomaterials show: by entering nano-scale, material science enters a non-scalable regime – nanomaterials do not behave like smaller units of bulk material, but inherently different.

Therefore, Vollath approves of the following definition of nanomaterials:

> *Nanomaterials are materials whose smallest building block has a size lower than 100 nm (in at least one dimension) and whose properties are directly associated with their small size* [31].

Pagliaro extends the discussed range to the entire sub-micron regime [30]. Phenomena of nano-scalation are not limited to one class of materials, they occur in metals, polymers, ceramics and particularly in case of composites that combine different material types. This is the case for a vast number of biological materials: bioceramics such as nacre, bone or tooth are composites of brittle minerals and soft proteins. They exhibit a similar stiffness as ceramics, but are several orders of magnitude tougher [32, 31].

Nanomaterials also differ from bulk material in terms of chemical behaviour. On the one hand this is favourable for the development of new powerful catalysts, on the other hand, the toxicity of nanoparticles is not yet fully studied and first results are alarming [33, 34, 35]. Contrary to bulk material, toxicity is closely linked to the structure and specific surface of the particles and conclusions from in-vitro studies can not easily be transferred to in-vivo studies. Therefore, Yildirimer et al. as well as Pagliaro urge the need for a standardised process of testing nanotoxicology to avoid the risk of unforeseen consequences [35, 30]. A responsible risk management from the early stages would also help overcoming public aversion and strengthen the position of nanotechnology on the long run [30].

Another challenge is the fabrication of nanomaterials. If a nano-scaled filler is dispersed in a polymer matrix, two main difficulties occur: (a) the dispersion of the filler particles and (b) the compatibility of matrix and filler. Different techniques to address problem (a), such as mixing in polymer-melt or dispersion of nanoparticles in the monomer before polymerisation, are summarized by Jordan et al. [36]. The underlying physical principle is the particles' high surface energy. It is reduced by the undesired formation of agglomerates. This phenomenon draws effort in primary fabrication of the particles as well as in further processing [31].

Compatabilisation (b) of matrix and filler is a task which already has to be addressed for conventional, micron-scale fillers, which are of high economic relevance for polymer and rubber industry [37]. Mineral fillers are mainly polar and need to be compatibilised with the unpolar matrix, otherwise they decrease toughness as they introduce defects [38]. Therefore, surface modifications of inorganic particles have been a vivid field of interest, and get even more relevant for nanoparticles [39].

Due to significantly higher fabrication costs compared to conventional materials, only those nanomaterials exhibiting outstanding behaviour are of scientific and economic interest [31].

2.2.2 Silica nanoparticles

Silicon dioxide (SiO_2) is the most commonly found inorganic substance on earth. It is highly inert as it can not be dissolved in acids except for hydrofluoric acid and is also resistant to alkaline media. It forms 3-dimensional networks, which are either amorphous or crystalline. Its most common

configuration is the polymorphic quartz. Silicates, the derivates of silicic acid ($Si(OH)_4$), represent the most important group of rock forming minerals [40].

Silica have been economically important since ancient times. Today, they are an irreplaceable raw material for nearly all domains of industry: whilst the wightwise largest part goes to the construction sector for cements, SiO_2 is also the main raw material for glass and silicon production and an additive for food, paper, cosmetic and medical applications [41]. In polymer industry, micro- and nano-structured silica and silicates play an important role as fillers.

Nano-silicates and nano-silica should not be confused: The manifold natural shapes of nano-silicates, especially those with high aspect ratios, are exploited for nano-structurisation. For example, layered silicates are used to obtain nacre-like structurs or to augment the electrical or diffusion barrier [42]. The main task lies in exfoliating and compatibilising the naturally grown structures [31]. Their application was studied for polyurethane elastomers amongst others [43].

On the contrary, amorphous silica, apart from fossil diatomaceous earth, is synthetically produced [44]. Selected processes to obtain amorphous silica are described below:

Precipitation process The main part (75 %) of amorphous silica is fabricated via the relatively cheap precipitation process. Herein, SiO_2 is formed from a solution of soluble silica (water glass) by the addition of sulphuric acid [44]. Usually particle sizes surpass 10 µm, however, methods have been found to form nanoparticles as well [45, 46].

Flame process Flame processes were a well established method to obtain pigments already before the rise of nanotechnology. Fumed silica, titania and carbon black are produced this way. In the basic process, a precursor, such as silan (SiH_4), silicon tetrachloride ($SiCl_4$) or a siloxane, is blown into a stable methane flame. Under these conditions the precursor is oxidised and silica particles form: their diameters decrease, the hotter the flame and the shorter the time passed in the flame are. However, smaller particles tend to form undesired fractal agglomerates. A certain variation of the temperature in the flame is inevitable. Therefore, it is not possible to form uniform particles. By application of an electric field, the time in the flame can be reduced as the newly formed particles carry charges due to thermal ionisation [31].

Stöber process In 1968, Stöber, Fink, and Bohn developed a method to produce spheric silica nanoparticles of small size distributions. In this process, alkyl-silicates undergo a hydrolysis with water to form $Si(OH)_4$ and ethanol. In the next step, the silicic acid condensates to form SiO_2 structures. The alkyl-silicates are dispersed in alcohol

and water; ammonia is added as morphological catalyst. By adaption of the concentrations, Stöber was able to vary particle sizes from 50 nm to 2 µm [47]. The Stöber process was further studied in terms of kinetics. Moreover, it was used to attain different structures, for example hollow or mesoporous nanoparticles. Thus, the condensation takes place on polymeric substrates [48].

Today silica nanoparticles are already applied in chemical surface polishing [49], cosmetics [30], varnishes and food stuffs (classified as E551)[50]. Large effort is taken on the introduction as carrier for the distribution of medicals in the body (nano-medicine) and as contrast agents for biomedical imaging [48].

Despite the promising advantages of the use of silica nanoparticles, their impact on health and environment has to be kept in mind, especially in medical and cosmetic applications. The toxicity of nanoparticles is a vivid field of research, however, the work is described as uncoordinated and far from being concluded [51]. The results depend on the production method, structure, size and dose of the nanoparticles as well as on in-vitro or in-vivo application. This leads to contradictory results and impedes general conclusions [48]. Indications for cyclotoxicity to liver, lung and blood cells were found above certain concentrations of silica nanoparticles [34]. A possible reason is the formation of oxygen radicals on the surface of silica nanoparticles [51]. Amongst others, Holl [34] and Albrecht, Evans, and Raston [51] reviewed findings on this area. They emphasise the necessity of special regulations for the admission of nanomaterials and standards for the evaluation of health and environmental hazards. Liberman et al. come to the conclusion that due to the relatively low toxicity silica nanoparticles have a high potential for medical applications [48].

2.2.3 Modification of silica nanoparticles

Surface modification of nanoparticles serves different aims. Firstly, agglomeration of nanoparticles can be hindered to sustain their size-dependant properties [52]. Secondly, in case of nanocomposites, the importance of compatibilisation with matrix material has already been emphasised in chapter 2.2.1. Depending on the requirements, this is either effectuated by physical compatibilisation or by covalent bonding to the matrix material. Moreover, silica nanoparticles are studied as substrate to immobilise or encage bioactive groups for therapeutical or analytical purposes [52, 53].

Surface modification can be reached via two different procedures, either grafting or co-condensation. For both procedures alkoxysilanes play a major role [54]. The particles used in this work were modified with one of the most common alkoxysilanes, (3-aminopropyl)triethoxysilane (APTES), whose structure is shown in figure 2.3.

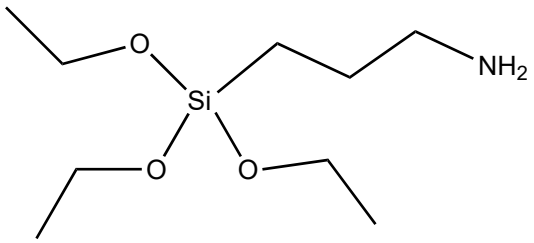

Figure 2.3: Structural formula of (3-aminopropyl)triethoxysilane (APTES)

In the grafting approach, a silanisation reaction as discovered by Bigelow, Pickett, and Zisman takes place: the ethoxy groups of APTES are substituted by the hydroxyl groups on the surface of the silica nanoparticles. The silicon of APTES gets integrated to the nanoparticle's structure whilst its organic chain is situated on the particle's surface. The reaction is conducted at ambient temperature by addition of water, ethanol and ammonia [55, 54].

The other modification route is co-condensation. Here, alkoxysilanes (for example APTES) are added to the precursors of the Stöber process (alkylsilicates) which are integrated in the nanoparticles upon particle formation. Therefore, the functional groups can be found on the surface as well as on the non-accessible interior of the nanoparticles [56].

2.3 Spectroscopic characterisation methods

Spectroscopic analysis methods have become irreplaceable tools for identification of molecular structures. Although the information obtained differs, the general underlying principle of measurement remains the same: interaction between electromagnetic waves and matter exhibit quantised characteristics. This is due to the fact that the transition from one state of matter to another, a quantised amount of energy is needed. This can be pictured as an energy gap.

The energy of an electromagnetic wave E is, according to equation 2.1, proportional to its frequency ν with the Planck's constant h as factor of proportionality.

$$E = h * \nu \tag{2.1}$$

Therefore, only waves of one specific frequency can surmount one specific energy gap. Light of this frequency will be absorbed when the sample is exposed to electromagnetic waves. On the contrary, light without any matching energy gap will be transmitted. Consequently, information about the molecular structure is obtained by the detection of the transmitted spectrum [18]. Two spectroscopic methods were used for analysis in this work: Fourier transform infrared spectroscopy (FTIR) and nuclear magnetic resonance spectroscopy (NMR).

2.3.1 Fourier transform infrared spectroscopy (FTIR)

When elements differing in electronegativity bind to each other, the bond has a dipole moment, which tends to adjust in an electric field. This is why the periodically changing electric fields of electromagnetic waves cause bonds to vibrate. The energy barrier to induce vibrations corresponds to specific wavelengths in the infrared region. Therefore, FTIR spectroscopy is a powerful tool, especially for characterisation of components containing groups of high polarity.

For translucent substances, infrared spectra can be measured in transmission (TR) mode, with a sensor capturing the wavelengths transmitted. The areas of low intensity represent characteristic absorption peaks. To analyse the surfaces of non-translucent and solid substances, the attenuated total reflection (ATR) mode is applied. The reflected light is analysed. Both methods have advantages and disadvantages. ATR has less restrictions on the materials which can be examined; contrarily to TR, the range of spectra are not limited by the transmittance of carrier plates and in general sample preparation is simpler. On the other hand, TR spectra have higher intensity resolutions and the chemical constituency of the entire liquid, not only its surface, is measured.

The obtained spectra show the intensity as a function of the wave number ($\tilde{\nu}$) in cm^{-1}. The wave number equals the inverse wavelength, which is the frequency divided by the speed of light. Typical FTIR spectra cover a region from 500 to 5000 cm^{-1} [57].

2.3.2 Nuclear magnetic resonance spectroscopy (NMR)

Nuclei of uneven mass numbers exhibit a property called spin. When exposed to a strong magnetic field[1], the spins adjust to it, either in parallel or anti-parallel position. There is a small energy difference between the two positions[2]. The energy (electromagnetic frequency) needed for a transition from one state to the other, depends on the electronic environment of the nucleus. For example, hydrogen atoms of ethane differ from ethylene in resonance frequency. As the frequency depends on the strength of the magnetic field, to attain non-machine-dependant values, the spectrum is normalised: the shift of the signal is measured compared to the signal of tetra-methyl silane and divided by the frequency of the spectrometer. The unit for this value, the chemical shift (δ), is parts per million (ppm). In general, all nuclei with uneven mass numbers can be used for analysis, the most common techniques are proton nuclear magnetic resonance spectroscopy (^{1}H-NMR) and carbon-13 nuclear magnetic resonance spectroscopy (^{13}C-NMR). ^{1}H-NMR has major advantages: as the ^{1}H isotope is the most frequent isotope of

[1] Common NMR devices operate at magnetic fields of 1.4 - 14 T

[2] in a range from 60 to 600 MHz, depending on the strength of the magnetic field

hydrogen, 99.98 % of the present hydrogen atoms contribute to the signal. Therefore, the number of scans and measurement time to attain spectra of high resolution is low. Furthermore, the integral of the peaks corresponds to the number of hydrogen atoms, which makes quantitative analysis possible. For the analysis of complex structures, a combination of ^{1}H-NMR and ^{13}C-NMR gives 2-dimensional spectra, that clarify which hydrogen atoms bind to which carbon atoms [19, 58].

Chapter 3

Experimental

3.1 Acrylation of PTHF

3.1.1 Used substances

Polytetrahydrofuranes (PTHF) with acrylate end-groups were necessary intermediate products to form nanocomposite structures. Although the synthesis process is described in literature [14, 15, 16], they are difficultly available on a commercial basis. Therefore, it was necessary to perform synthesis in order to obtain the required substances. PTHF of various molecular weights of BASF's product portfolio PolyTHF® were used:

- polytetrahydrofurane (M=250 g/mol) (PTHF250)
- polytetrahydrofurane (M=1000 g/mol) (PTHF1000)
- polytetrahydrofurane (M=2000 g/mol) (PTHF2000)
- polytetrahydrofurane (M=2900 g/mol) (PTHF2900)

The second reaction partner for the esterification reaction, acrylic acid, was supplied by Sigma Aldrich. The reaction was performed in cyclohexane, hydroquinone (1,4-benzenediol) as polymerisation inhibitor and p-toluene sulphonic acid (p-TSA) as catalyst were added. Those compounds were supplied by Sigma Aldrich as well.

Furthermore, the following reactants for quenching and purification were supplied by Carl Roth: potassium carbonate (K_2CO_3), sodium hydroxide (NaOH) and sodium sulphate (Na_2SO_4).

The products of the reaction, acrylated polytetrahydrofuranes, are referred to as PTHF250ac, PTHF1000ac, PTHF2000ac and PTHF2900ac.

3.1.2 Used apparatus

In a first step, the reaction was performed on a small scale in a 500 ml three-necked round flask (apparatus 1) and later extended to a 2 l reactor

(apparatus 2) to produce larger quantities. In both setups, the reactors were connected with a Dean-Stark receiver which led to a reflux condenser.

In the course of the esterification reaction, water is formed. It is insoluble in cyclohexane in liquid state. However, the mixture shows azeotropic characteristics. This means, the concentration of the vapours equals the concentration of the liquid. Cyclohexane evaporates at its boiling temperature of 80.738 °C [59] and entrains water present in the reaction mixture. When the vapour condensates at the reflux condenser, the liquids separate and the denser water sinks to the bottom of the boiling trap of the Dean-Stark receiver. The reaction progress can be controlled by the height of the water's meniscus in the trap.

The reaction was heated in an oil bath at 120 °C and stirred with a magnetic stirrer for apparatus 1. Apparatus 2 was heated in a water bath at 95 °C and stirred with a sealed precision glass (KPG) stirrer with a plate made of polytetraflouroethylene (PTFE). The temperature was limited by the azeotrope's boiling temperature. To minimise heat losses and losses of water as heat medium, the apparatus was isolated with aluminium foil. The loss of water was compensated by refilling the water bath with approximately 1 l/8 h. Instead of lubricants, PTFE collars were used at the connections between the glass instruments to avoid contamination.

For quenching and cooling, separation funnels and flasks were needed. In a last step, the product was separated using a rotary evaporator (Heidolph Laborota 4000). In one purification setup a vacuum oven (Binder VDL) was used.

3.1.3 Procedure

Synthesis

The molar relations of the components were derived from literature [14] and are shown in table 3.1. The basic mixture contained acrylic acid in an excess of 30 %.

Table 3.1: Composition of reaction mixture for acrylation reactions (solvent: cyclohexane

substance	molar parts
PTHF	1.00
acrylic acid	2.60
hydroquinone	0.15
p-toluene sulphonic acid	0.03

Hydroquinone is well-known to act as an antioxidant. Due to its aromatic structure it is able to transform reactive radicals into resonance-stabilised

radicals [19]. Therefore, it inhibits radical polymerisation of the acrylate double bond in acrylic acid. When treated with an alkaline solution, it undergoes a non-reversible change of colour from translucent to a strong dark brown. Therefore, after alkaline quenching of the reaction the product's colour indicated the quality of purification. The amount of cyclohexane was adapted to the size of the reaction vessel. In apparatus 1 approximately 300 ml were used, in apparatus 2 600 ml cyclohexane were added. The esterification reaction is catalysed by p-TSA. The advantage of this common acidic catalyst lies in its non-oxidising behaviour.Before adding the catalyst, the reaction mixture was heated and homogenized for 30 min to ensure stable conditions. The liberated amount of water was calculated by the following formula, whereby m indicates the mass and M the molar mass of the components:

$$m_{H_2O} = \frac{M_{H_2O}}{M_{PTHF}} * 2 * m_{PTHF} \tag{3.1}$$

The results of this calculation were taken to monitor reaction progress and to determine whether the conversion was completed and the mixture was ready for quenching. In table 3.2, the results of this calculations are listed and compared to the amount of water measured before quenching at time t. For PTHF1000 and PTHF2000, the reaction progress was additionally monitored by FTIR (ATR) of the reaction mixture.

Table 3.2: Parameters of reaction conditions for acrylations of PTHF

M_{PTHF} [g/mol]	m_{PTHF} [g]	$m^{calc}_{H_2O}$ [g]	m_{H_2O} [g]	t [h]
250	40	5.8	5.2	9
2000	40	0.7	–	9
1000	800	28.8	27.0	78
2000	800	14.4	13.2	75
2900	800	9.6	8.2	130

To accelerate the reaction, additional acrylic acid and catalyst were added at later stages. As this did not have any obvious impact, the approach was not pursued any further.

Purification

To remove acidic and polar reactants it was necessary to quench the reaction mixture under alkaline conditions. Hence, aqueous components were introduced to the non-polar mixture. This led to an incomplete phase separation, whereby the intermediate phase was larger and more stable the higher the molar mass of the PTHF used. More precisely, for PTHF250 no interme-

diate phase was formed. On the contrary, most of the aqueous volume of PTHF2000 mixture was occupied with the intermediate phase.

A large part of the product formed this sponge-like sludge in the aqueous phase. Not exploiting it would have caused unsupportable yield losses. Therefore, another purification procedure had to be developed. Compared to the substances derived when applying the purification procedure proposed in by Guan et al., a higher level of purity was attained [14].

In this work, three different procedures were studied which exhibited differences in the state of quenching media and in the method to remove aqueous components. Method A was the one suggested in literature [14]. Method B differed significantly from method A and led to the development of the most effective method C. All three methods will be described in detail in the following:

Method A: The quenching was effectuated by adding solid K_2CO_3 at reaction temperature and stirring the mixture without heating over night. In the next step the mixture was filtered with filter paper at the application of a Büchner funnel. Later, the solvent was removed using the rotary evaporator at 40 °C and a reduced pressure of 235 mbar. When most of the solvent was evaporated, the pressure was decreased to 180 mbar. Finally, the product was transferred into a separation funnel and extracted with NaOH solution (c_{NaOH}=1 mol/l). At this stage, the hydroquinone led to a colour change of the organic phase from slightly yellowish to strongly brownish. The mixture was shaken until clarification of the organic phase. The process was repeated using water instead of the alkaline solution to remove the alkaline components. The organic phase was separated and dried in a vacuum oven for 2-3 days at a temperature of 40 °C[1].

Although the problems caused by phase separation were less severe than in the other methods, a number of disadvantages of this method must be emphasised:

- Loss of product in the filtering step
- Solid contamination by small particles of K_2CO_3 which were still present in the final product
- Colouring of the final product which might be due to impurities
- Risk of incomplete drying

Method B: The reaction mixture was filled into a separation funnel and saturated K_2CO_3 solution was added for quenching. Besides the formation of carbon dioxide (CO_2), this led to an immediate change of

[1]It was found not advisable to increase the oven temperature to accelerate drying, as at a temperature of 80 °C degradation and curing were observed.

colour as in method A. The mixture was further purged with NaOH solution (c_{NaOH}=1 mol/l), which led to the formation of the previously described stable intermediate phase. The following measures were taken to facilitate phase separation:

- The temperature of the fluid was raised to 50 °C by placing the separation funnel into an oven.
- Sodium chloride NaCl was added to increase the polarity of the inorganic phase.
- n-Hexane was added to decrease the organic phase's polarity.

Whilst the first two measures reduced but did not completely dissolve the intermediate phase, the addition of n-hexane strongly improved the process. The organic phase was separated and the solvents were removed by rotation evaporation to obtain a translucent and slightly yellowish product.

Method C: Taking into account the observations from method B, its procedure was optimised to obtain the final method C. In this method, the reaction mixture was diluted (1:1) with n-hexane before quenching the reaction with saturated K_2CO_3 solution[2]. The aqueous phase was removed and NaOH solution (c_{NaOH}=1 mol/l) was added. The formed intermediate phase was less pronounced than in case of application of method B. The organic phase was separated and rinsed until complete discolouration was reached. The solution was dried in the presence of Na_2SO_4 for one hour. Karl Fischer titration did not detect a change of water content (0.018 %). This is why the drying step is not considered necessary. The product was obtained by evaporation of the solvent. The beforehand separated intermediate phase was diluted with n-hexane (1:1). The product diffused into the organic phase, which was treated like the organic phase after the first separation.

Characterisation

The products were characterised via the following methods:

- FTIR spectroscopy in TR or ATR mode. 72 scans were performed per measurement. In TR the sample was placed between two calcium fluoride (CaF_2) plates.
- ^{1}H-NMR of a sample of 10 mg dissolved in deuterated chloroform. The degree of conversion was calculated by comparing the integrals of the protons neighbouring the newly formed acrylates (between 5.7 and 6.5 ppm) with the ether peak at 3.39 ppm.

[2]This again requested a careful treatment due to the formation of CO_2.

- The hydroxyl values HV of PTHF1000 and PTHF1000ac were determined to acquire further information on the conversion rate. The hydroxyl value (HV) expresses the content of free hydroxyl groups in a material.[3] The amount of sample required can be calculated by formula 3.2, on behalf of the expected HV.

$$m = \frac{450}{HV} \tag{3.2}$$

It is evident that the method requires large amounts of sample for substances of small HV. Therefore, it was not feasible to repeat it for PTHF2000ac and PTHF2900ac. For the analysis of PTHF1000ac, an amount of 45 g was used.

The HV is a widely applied value in polyurethane processing. It was determined by the following procedure: the examined polyol was esterificated with 20 ml of a solution of phthalic anhydride (PA) in pyridine (c_{PA}=1 mol/l). The reaction mixture was boiled with a reflux condenser for one hour. In the next step, 20 ml water and 40 ml isopropyl alcohol were added. The amount of KOH solution (c_{KOH}=1 mol/l) needed for its neutralisation was determined by titration. A blank feed without any polyol added underwent the same procedure. The amount of hydroxyl groups per gram polyol was derived from the difference of the amount of KOH needed between the blank feed and the sample, according to equation 3.3. The variables are explained in table 3.3.

$$\mathrm{HV} = \frac{M_{\mathrm{KOH}} * (V_S - V_{BF}) * c_{\mathrm{KOH}}}{m_S} \tag{3.3}$$

Table 3.3: Variables used in equation 3.3

M_{KOH}	g/mol	molar mass of KOH
V_S	ml	volume of KOH solution needed to neutralise the sample
V_{BF}	ml	volume of KOH solution needed to neutralise the blank feed
c_{KOH}	mol/l	concentration of KOH solution
m_S	g	mass of the examined sample

[3] More precisely it is defined as the mass of potassium hydroxide (KOH) in mg equivalent to 1 g of the sample in its ability to bind to phthalic anhydride. Therefore, the amount of hydroxyl end-groups per mol PTHF is determined by dividing the HV by the molar mass of KOH and multiplying it with the molar mass of the investigated PTHF.

3.2 Characterisation of silica nanoparticles

3.2.1 Used substances

The nanoparticles investigated in this part were supplied by IoLiTec GmbH and specified as *silicon oxide+amino group (6:1) 99,8 %* (NO-0056-HP). The average particle size ranges between 10 and 20 nm and the particles' specific surface area amounts to 90-130 m^2/g, according to the supplier. Silica nanoparticles without modification supplied by Sigma Aldrich were characterised for reference purposes.

Titrations were performed with hydrochloric acid (HCl) (c_{HCl}=0.1 mol/l) and p-toluene sulphonic acid (p-TSA) ($c_{p\text{-}TSA}$=0.1 mol/l). Phenolphthalein was used as indicator. All chemicals were supplied by Sigma Aldrich.

3.2.2 Used apparatus

For titrations, a laboratory centrifuge, common burettes and a magnetic stirrer were used.

For thermogravimetric analysis (TGA), Mettler-Toledo TGA/DSC-1 of the Chair of Chemistry of Polymeric Materials, Montanuniversität Leoben, was used.

As the equipment for two analytical methods was not available at the Montanuniversität Leoben, those measurements were ordered from partner institutes: firstly, DLS was performed at the Institute for Inorganic Chemistry of the Technical University of Graz (TU Graz) with an equipment consisting of a diode laser Coherent Verdi V5 and a goniometer with single-mode fiber detection optics (OZ from GMP, Zürich, Switzerland). The laser ray had a wavelength (λ) of 532 nm and a maximum power (P_{max}) of 5 W [60]. Secondly, elemental analysis was performed in the microanalytical laboratory of the Faculty for Chemistry of the University of Vienna [61].

3.2.3 Procedure

In the titrations performed, amine-modified silica nanoparticles were dispersed in HCl solution (c_{HCl}=0.1 mol/l). The alkaline amine groups reacted with the acid and therefore rendered the solution less acidic. By titration with KOH solution (c_{KOH}=0.1 mol/l), the amount of reacted HCl was detected. Practically, the particles were dispersed in 50 ml HCl solution and stirred for 30 minutes to ensure complete conversion. In the next step, this primary solution was centrifuged to ensure sedimentation of the particles. 4 samples of 10 ml were taken, 3 drops of phelolphthalein were added and the solution was titrated with KOH solution (c_{KOH}=0.1 mol/l) until the indicator changed colour. This procedure was effectuated for a blank feed, a sample containing 0.5, 1, 1.5 and 2 g amine-modified silica nanoparticles (SiO_2–NP+NH_2). The amount of amine groups per gram nanopar-

ticles was calculated according to equation 3.4. For the titration series with HCl the result is an average value of 16 measurements.

$$f = \frac{(V_{KOH}^{BF} - V_{KOH}^{S}) * c_{KOH}}{1000 * m_{NP} * \frac{V_{HCL}}{V_{HCl}^{0}}} \tag{3.4}$$

Table 3.4: Variables used in equation 3.4

f	mol/g	functionality of nanoparticles in mol amine-functional groups per gram SiO_2–NP+NH_2
V_{KOH}^{S}	ml	volume of KOH solution needed to neutralise the sample
V_{KOH}^{BF}	ml	volume of KOH solution needed to neutralise the blank feed
c_{KOH}	mol/l	concentration of KOH solution
m_{NP}	g	mass of nanoparticles dispersed in primary HCl solution
V_{HCl}^{0}	ml	volume of primary HCl solution
V_{HCl}	ml	volume of sample taken from primary HCl solution

In a next series, the procedure was repeated for dispersions of 1.25, 1.875 and 2.5 g nanoparticles per 50 ml p-TSA solution ($c_{p\text{-}TSA}$=0.5 mol/l). The result is an average value of 11 measurements.

In TGA, approximately 10 mg of the particles were filled into a ceramic analysis crucible, tempered at 25 °C for 5 minutes. Then the temperature was increased 5 K/min until 150 °C were reached. This temperature level was held for 30 minutes to evaporate water and low molecular weight substances. During the next heating ramp of 5 K/min until a temperature of 1000 °C the weight loss was related to oxidation of organic groups. The analysis took place in oxygen atmosphere.

Dynamic light scattering measurements were performed at TU Graz. Particles were dispersed in ethanol. The analysed samples had a dilution ratio of 1:20. Some samples contained large aggregates, which would have exceeded the resolution of the method. After their sedimentation (approximately 5-10 minutes), the measurement was conducted with the serum above the sedimented particles.

3.3 Aza-Michael reaction

3.3.1 Used substances

A major part of this work is dedicated to the question, if and under which conditions acrylated PTHF is able to act as Michael acceptor in aza-Michael

reactions. Therefore, a series of model substances and various catalysts were needed:

Michael acceptors: 1,4-butanediol diacrylate (BDODA), supplied by Sigma Aldrich, as the smallest homologous unit of PTHF was studied before turning to the synthesised polytetrahydrofurane (M=1000 g/mol, acrylic terminating groups) (PTHF1000ac)

Michael donors: Most of the model reactions were conducted using decylamine supplied by Sigma Aldrich. Being a primary aliphatic amine, decylamine is supposed to be a good model for primary aliphatic amines on amine-modified nanoparticles. Moreover, macromolecular Jeffamine® D polyetheramine (M=430 g/mol) supplied by Huntsman was studied in an additional series.

Catalysts: Besides water, $AlCl_3$ functionalised silica gel and $AlCl_3$ (supplied by Sigma Aldrich), as well as boric acid (H_3BO_3) and cerium(IV) ammonium nitrate (CAN) (supplied by ABCR) were studied as catalysts.

Furthermore, the deuterated chloroform required for ^{1}H-NMR analysis was supplied by Sigma Aldrich as well as the pure ethanol, which was used as solvent in certain experiments.

3.3.2 Used apparatus

In general, aza-Michael reactions were performed in 20 ml glass vials stirred on a magnetic stirrer. For one catalysis series, a common household microwave oven (Severin) was used. Furthermore, one experiment required a simple laboratory setup consisting of a heater, a round flask and a reflux condenser.

Spectroscopic analyses were conducted at the Chair of Chemistry of Polymeric Materials, Montanuniversität Leoben, using Bruker Vertex 70 FTIR spectrometer and Varian 400 MR NMR spectrometer.

3.3.3 Procedure

Before focussing on decylamine as amine model substance, a few reactions were performed with Jeffamine® D polyetheramine (M=430 g/mol) (Jeffamine® D 400) as amine-containing species. 1,4-butanediol diacrylate (BDODA) and PTHF1000ac served as Michael donors. Pure $AlCl_3$ was used as catalyst, which later was not considered an ideal approach, due to its reactivity that caused side reactions. 10 mmol (2 g) of BDODA and 10 mmol of Jeffamine® D 400 were brought to reaction. No catalyst, 0.8 mmol (0.1 g) and 2.2 mmol (0.3 g) $AlCl_3$ were added. All products were characterised using FTIR spectroscopy.

To investigate the effectiveness of selected catalysts, aza-Michael reactions with decylamine formed the major part of this work. In a first series, various catalysis paths were studied for a reaction between BDODA and decylamine. The composition of this series is listed in table 3.5 below. The stoichiometric relation between the bifuntional BDODA and the monofunctional declyamine is 1:2.

Table 3.5: Composition of series 1: BDODA + Decylamine

BDODA		Decylamine		Catalyst		
[mmol]	[g]	[mmol]	[g]		[mmol]	[g]
0.5	0.099	1	0.157	$AlCl_3$ on silica gel	0.3	0.2
0.5	0.099	1	0.157	H_2O	55.5	1.0
0.5	0.099	1	0.157	H_2O+microwave	55.5	1.0
0.5	0.099	1	0.157	0.3 M H_3BO_3 solution	0.3	1.0
0.5	0.099	1	0.157	0.3 M CAN solution	0.3	1.0

The amount of catalyst used is based on literature: Saidi, Pourshojaei, and Aryanasab successfully catalysed various aza-Michael reactions of low-molecular reactants with 0.2 g of silica-supported $AlCl_3$ per mmol reactant at 60 °C [28]. Ranu and Banerjee described the accelerating effect of water at room temperature for Michael reactions of primary and secondary amines with methyl acrylate and other low-molecular Michael acceptors [62]. Kall, Bandyopadhyay, and Banik supposed effective use of microwave treatment to enhance conversion rate and reaction time [63]. Furthermore, aqueous solutions of H_3BO_3 ($c_{H_3BO_3}$=0.3 mol/l) or CAN (c_{CAN}=0.3 mol/l) are described as effective catalysts [27, 29].

For all cases of aqueous solutions, 1-1.5 mmol of Michael acceptor and 1 mmol of Michael donor were added to 1 ml of water or aqueous solution.

BDODA was expected to behave similarly, being a homologous species to the acrylated PTHFs. However, due to the difference in molecular weight, transferring conclusions was difficult. So a second series to study different catalysts for PTHF1000ac and decylamine was needed. The composition of this series is shown in table 3.6.

Table 3.6: Composition of series 2: PTHF1000ac + Decylamine

PTHF1000ac		Decylamine		Catalyst		
[mmol]	[g]	[mmol]	[g]		[mmol]	[g]
1	1.1	1	0.157	H_2O	55.5	1.0
1	1.1	1	0.157	H_2O+microwave	55.5	1.0
1	1.1	1	0.157	0.3 M H_3BO_3 solution	0.3	1.0
1	1.1	1	0.157	0.3 M CAN solution	0.3	1.0

As the organic reactants are not fully soluble in water, the reaction mixture remained inhomogeneous, which caused difficulties for its characterisation: FTIR measurements were little conclusive and no NMR scans were performed. An additional series was started to further investigate on the reaction catalysed with CAN solution, which differed from the others by forming an insoluble product. However, the reaction has not yet been understood.

Referring to the results of series 2, the most promising results were observed under aqueous conditions. Therefore, this catalysis method was chosen to be pursued for a reaction in ethanol solution. As PTHF1000ac is soluble in ethanol, the homogeneous reaction mixture was suited for NMR analysis. The following preparation technique was used: 10 ml ethanol were added to the equivalent composition of decylamine and PTHF1000ac as in series 2 (3.6). After dissolving, 1 ml of water was added as catalyst. One sample was heated in the microwave oven for 15 s, one was kept at room temperature, one was heated in a reflux condenser for 2 hours. Due to circumstances, ^{1}H-NMR measurements were only possible 14 days after the reaction, which led to equivalent results for all samples. Only the samples with microwave-induced heating were repeated to gain time-dependant results. Furthermore, in this series, the solvent was removed with a rotatory evaporator for higher resolutions. Those samples were investigated more closely , via additional ^{13}C-NMR, two-dimensional NMR and FTIR, to find out the reaction products' nature.

To conclude and bring together the different work packages of this thesis, it was tried to perform a first Michael reaction on silica nanoparticles. The composition consisted of 0.5 g amine-modified silica nanoparticles, 1.1 g PTHF1000ac, 1 ml water as catalyst and 10 ml ethanol. The mixture was heated in the microwave oven for 15 s and ^{1}H-NMR measurements were performed in deuterated chloroform after one hour as well as after five days.

Chapter 4

Results

4.1 Acrylation of PTHF

4.1.1 Products

After purification, acrylated polyols were clear, yellowish, viscous liquids. Samples prepared according to method A tended to crystallise, most probably impurities acted as nucleation agents and initiated crystallisation. Samples prepared according to method C remained liquid even one year after synthesis; no changes in chemical composition were detected via FTIR spectroscopy over time. The acrylated polyols offer a series of newly formed groups which can be easily detected via FTIR and ^{1}H-NMR spectroscopy.

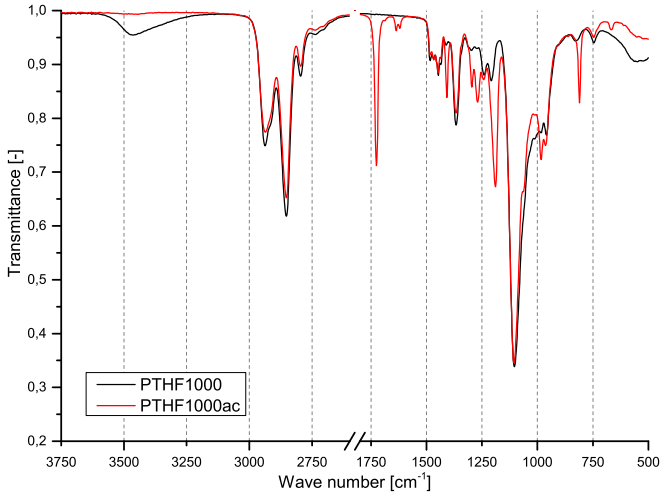

Figure 4.1: FTIR spectra of PTHF1000 and PTHF1000ac

The hydroxyl peak in FTIR scans ($\tilde{\nu}$=3600-3200 cm_1) was eliminated and simultaneously several new peaks appeared, which are related to the acrylate group (CH_2=CH_2-C(=O)-O-). The spectra indicated that the acrylates were covalently coupled to the polyols and did not belong to remaining acrylic acid (educt), as the newly appeared C=O stretching vibration in acrylate esters differed from C=O stretching vibration of carboxylic acids. As an example, the spectra of PTHF1000 and PTHF1000ac are compared in figure 4.1 and the interpretation of the peak frequencies is listed in table 6.1 in the appendix. The spectra of reactions of polyols with different molar mass are provided in the appendix (figure 6.1, 6.2, 6.3). All spectra are in line with each other, they also match with BDODA (see figure 6.4)(except for the groups of the polyether backbone). This is illustrated in figure 4.2, which shows the similarities of the FTIR spectra between the homologous series of products synthesised.

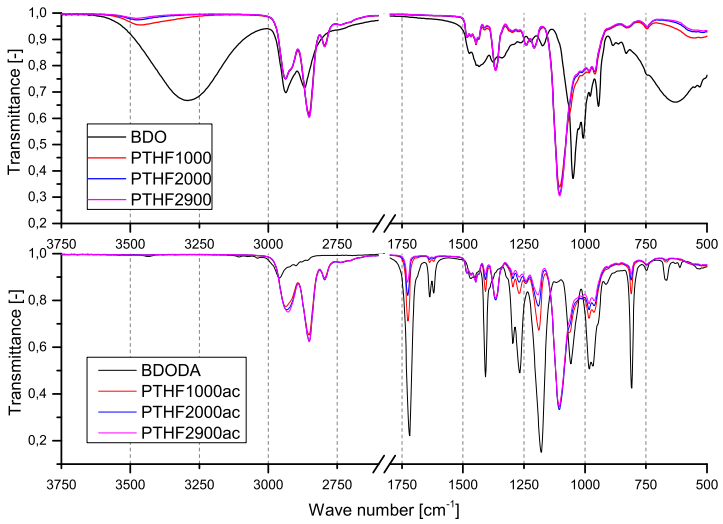

Figure 4.2: FTIR spectra of polyols and acrylated polyols of different molar masses

In the ^{1}H-NMR spectra of PTHF only 3 different kinds of hydrogen atoms are visible, all of them belonging to methylene groups: those bonded to the ether bond (δ = 3.39 ppm), their neighbouring carbon atoms (δ = 1.60 ppm) and those bonded to the hydroxyl end-groups (δ = 3.61 ppm). The structural formula of PTHF is shown in figure 4.3, including its ^{1}H-NMR shifts. The molar mass of the different types of PTHF is an average value for the mass distribution. The number of repeating units (n) varies. The calculated amount of ether units for the given molar mass are listed below (see table 4.1). H_{th} refers to the theoretical number of hydrogen atoms at

the given chemical shift δ.

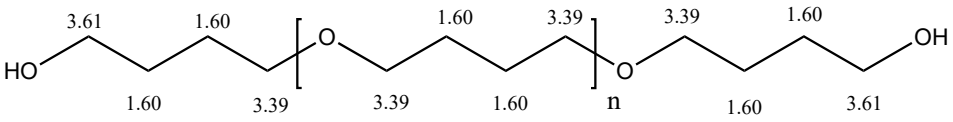

Figure 4.3: Structural formula of polytetrahydrofurane (PTHF) including ^{1}H-NMR shifts

Table 4.1: Stoichiometric relations of PTHF

	M [g/mol]	n	H_{th} $\delta = 3.39$	H_{th} $\delta = 1.60$
PTHF1000	1000	12.6	50.4	54.4
PTHF2000	2000	26.5	106	110
PTHF2900	2900	39.0	156	160

Due to the distribution of molar mass, the quantitative calculation of hydrogen atoms did not necessarily reach even numbers. To gain awareness for this phenomenon, the stoichiometry of PTHF educt was studied by ^{1}H-NMR. The results are listed in table 4.2.

For PTHF2900 the amount of hydroxyl groups measured in ^{1}H-NMR was by 25 % less than expected. Two explanations were found: firstly, if the molar mass of the substance was higher than specified or secondly if some PTHF molecules contained non-reactive end-groups. However, due to the broadness of the peaks, the analysis of peak areas exhibited an uncertainty. This has to be kept in mind, when deriving conversion rates from ^{1}H-NMR spectra of the acrylated products.

The ^{1}H-NMR spectra of the products of acrylation confirmed the findings of FTIR spectroscopy. New peaks, corresponding to the hydrogen bonded to the acrylate group and the ester group appeared. Quantitative analysis turned out to be difficult for the following reasons: the hydrogen atoms bonded to the acrylate group should all account to the same value, however

Table 4.2: ^{1}H-NMR-shifts of characteristic groups in PTHF

δ [ppm]	δ_{ref} [ppm]		PTHF1000 H	PTHF1000 H_{th}	PTHF2000 H	PTHF2000 H_{th}	PTHF2900 H	PTHF2900 H_{th}
3.61 tr	3.64[58]	-C**H$_2$**-OH	3.96	4	4.01	4	3.51	4
3.39 brs	3.40[16]	-O-C**H$_2$**	50.39	50.4	105.25	106	155.7	156
1.60 brs	1.60[16]	-C**H$_2$**-	54.4	54.4	110	110	160	160

their integrals varied by 10 %. For the calculation of conversion rates, constant reference peaks were necessary. The only constant peaks present were those of the macromolecular backbone. Not only were they broad and risked to incorporate other peaks, their reference value was uncertain as well, due to the mass distribution.

Nevertheless, the values indicated that the acrylation of PTHF was conducted successfully. The spectra as well as the interpretation of the peaks are depicted in the appendix: for PTHF1000 see table 6.2 and figure 6.5, for PTHF2000 see table 6.3 and figure 6.6 and for for PTHF2900 see table 6.4 and figure 6.7.

The integrals of the newly formed peaks were calculated using the ester peak as a constant reference. These values (H) were compared with the theoretical amount of hydrogen atoms for total conversion (H_{th}). The derived degree of conversion ranged between 72 and 85 % for PTHF1000 and PTHF2000. Surprisingly, conversion rates of PTHF2900 were between 80 and 100 %. This might be due to the prolonged reaction time.

A third method that supported the results was ^{13}C-NMR. To predict the chemical shifts, ChemDraw software was used. Spectra of the products are shown in the appendix: For PTHF1000ac see figure 6.8, for PTHF2000ac see figure 6.9 and for PTHF2900ac see figure 6.10. The peaks found were compared to the peaks predicted for PTHF in table 6.5 and for acrylated PTHF in table 6.6. Residuals of the solvent n-hexane were detected for PTHF2000ac and PTHF2900ac. The methylene groups detected in ^{1}H-NMR spectra belonged most probably to this solvent and did not indicate any side reactions.

For PTHF1000, the hydroxyl value (HV) of 112 before esterification was reduced to a value of 9.0 for PTHF1000ac. This indicated a conversion rate of 92 %.

After the determination of the chemical composition of the compounds synthesised, their thermal stability was analysed. Whilst the decomposition of PTHF led to one single weight loss step between 300 and 400 °C, the acylates showed two weight loss steps: firstly, between 100 and 200 °C a weight loss of 3-7 % and secondly compete decomposition between 350 and 450 °C. Most probably, the first step is related to volatile impurities (hexane, cyclohexane, water). The reason for the increased decomposition temperature might be the radical polymerisation of the acrylates. This was also indicated by the undesired curing of PTHF250ac during drying at 80 °C. Graphs of TGA analysis are shown in figures 6.11, 6.12 and 6.13 in the appendix.

To further investigate the decomposition process, pyrolysis gas chromatography – mass spectroscopy (GCMS) measurements were performed. However, the results were of low relevance and difficult to reproduce: It was not possible to detect acrylic acid as product of decomposition, as its molar mass was below the threshold of the method. At 200°C, next to no products were detected at retention times below 11 s; at 600°C decomposition was

more relevant. For example at 600 °C butanol acrylate, the product of bond rupture of the first ether bond was identified, which was not present at 200°C.

4.1.2 Reaction

The reaction progress of the acrylation of PTHF1000 and PTHF2000 was studied via FTIR spectroscopy of the reaction mixture. Educts and products were present as the samples were neither quenched nor purified. Over the course of the reaction, the peak of C=O stretching vibration in carboxylic acids ($\tilde{\nu}$=1715-1680 cm^{-1}) disappeared. Simultaneously, new peaks appeared. For evaluation, the $=CH_2$ twisting vibration ($\tilde{\nu}$=825-800 cm^{-1}) and the $=CH_2$ deformation vibration ($\tilde{\nu}$=1424-1393 cm^{-1}) were chosen. The evolution of these peaks over reaction time are shown in figure 4.4 for PTHF1000 and in figure 6.16 in the appendix for the acrylation of PTHF2000.

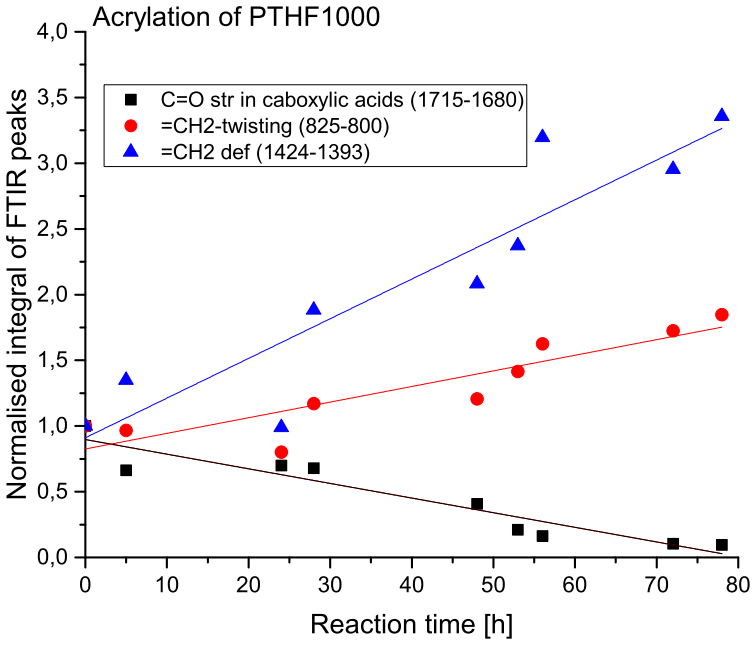

Figure 4.4: Graph of time-dependant normalised integral values of FTIR spectra of the reaction mixture during acrylation of PTHF1000

Intensity values of FTIR scans are sample-dependant, due to the contact surface conditions in ATR or sample thickness in TR mode. To eliminate these influences, it was necessary to divide the analysed integrals by the

integral of a group of constant concentration over the course of the reaction: the CH_2 backbone ($\tilde{\nu}$=3000-2850 cm^{-1}). To obtain the relative change of surface area, the normalised values were divided by the normalised integral value at the start of the reaction. The reaction of PTHF2000 showed worse correlation, this might be due to the attempt to accelerate the reaction of PTHF2000 by adding further acrylic acid before the last sample was taken.

4.2 Characterisation of silica nanoparticles

To prove the presence of amine groups on the nanoparticles, FTIR spectroscopy was performed. Compared to non-modified silica nanoparticles supplied by Sigma Aldrich, infrared signals were detected in the region $\tilde{\nu}$=3500-2500 cm^{-1} with a well-defined peak at 2929 cm^{-1} (see figure 6.17 in the appendix). This matched with literature values for absorption of primary amines as well as with the peak measured in decylamine [64].

The functionality of amine-modified silica nanoparticles was quantitatively determined by different methods. The average value of 15 titrations with HCl was 2.39 mmol/g with a standard deviation of 0.075 mmol/g. For the range of concentrations studied (0.05 to 0.2 g/ml) the functionality was independent of concentration. The series of titrations with p-toluene sulphonic acid (p-TSA) revealed lower functionalities: for 13 measurements, an average value of 1.71 mmol/g and a standard deviation of 0.19 mmol/g were calculated.

In TGA (see figure 6.18 in the appendix) two weight loss steps were measured. The first accounts most probably for water, as the particles were highly hygroscopic.[1] The second weight loss step arose from the decomposition of organic groups. When the APTES modification on the particle's surface decomposes, only the propylamine group (C_3H_8N) is oxidised and contributes to the weight loss. Silicone and oxygen atoms become part of the inorganic particle.

Therefore, the degree of functionality is calculated by dividing the weight loss per gram nanoparticles by the molar mass of propylamine (58 g/mol). In these calculations either the initial weight of the non-dried nanoparticles or the residual weight after the first weight loss step, can be applied. The value for non-dried particles should be taken for comparison with results of the other methods, as the titration measurements were also conducted with non-dried particles. The degree of functionality for non-dried particles amounts to 2.23 mmol/g; for dried particles a value of 2.24 mmol/g was determined.

The calculations of functionality from elemental analysis are based on the same considerations. The results of elemental analysis are the weight percentages of carbon, nitrogen and hydrogen. When APTES modified par-

[1] When a sample of particles was left at ambient atmosphere after drying in an oven (150 °C, 1 day), the weight increased by 3.5 % in 2.5 h.

ticles decompose, a propylamine group is oxidised. This group contains a well-defined amount of oxygen, nitrogen and hydrogen atoms. Therefore, the weight percentages were devised by the atomic mass of the element and the number of atoms of this element per propylamine unit. The average degree of functionality based on the nitrogen content was 2.051 mmol/g with a standard deviation of 0.003 mmol/g for 3 measurements. Based on carbon content, the degree of functionality was 2.38 $\pm$0.09 mmol/g. The surface of silica particles also contained hydroxyl groups which had not been modified, therefore, the elementary analysis for hydrogen was less relevant for the determination of functionality. This is why the calculated values were higher than those of any other method: 3.25 ± 0.09 mmol/g.

A diagram, comparing the results, is shown in figure 4.5. The titration using p-TSA gave the lowest degree of functionality. This could be explained by steric phenomena: whilst some amine groups might not be accessible for the protons associated with the p-toluene sulphonate counter-ion, the smaller chloride counter-ion is less hindering. The higher range of variation of p-TSA titrations supported this assumption, as it indicated further influences, which were not relevant for HCl titrations.

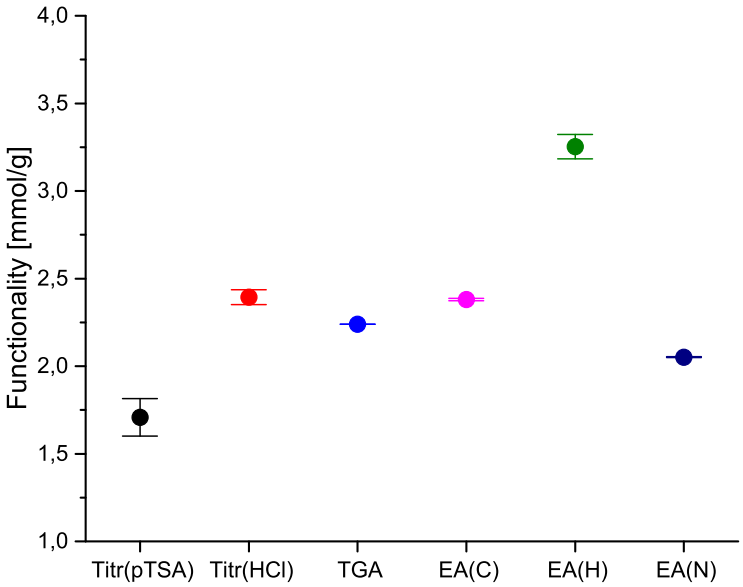

Figure 4.5: Degree of functionality of SiO_2–NP+NH_2 according to titrations with p-TSA and HCl, TGA and elemental analysis (EA) of carbon (C), hydrogen (H) and nitrogen (N)

To summarise, the functionality of IoLiTec amine-modified silica nanoparticles is between 2 and 2.5 mmol/g, although not all amine groups might be accessible for chemical reactions with bulky reactants.

The size of particles was examined by dynamic light scattering (DLS). The results are shown in figure 6.19 in the appendix. The distribution of the radii was broad: it ranged from 8 nm to 110 nm and had a maximum at a hydrodynamic radius of 54 nm. Non-modified silica nanoparticles were analysed as well. Their curve shifted to higher hydrodyamic radii with a maximum at 63 nm.

The hydrodynamic radius differed from the effective particle radius, due to solvent molecules attached to the particle surface. The particles were nano-scaled, however, their size had a wider distribution and was larger than specified by the manufacturer (10-20 nm). Moreover, particles exceeding the range of measurement (250 nm), probably agglomerates, were present.

4.3 Aza-Michael reaction

Before investigating the acrylated PTHF, preliminary studies were conducted with 1,4-butanediol diacrylate (BDODA) as a Michael acceptor. In a first series, Jeffamine® D 400 was used as an amine donor and $AlCl_3$ as a catalyst. FTIR measurements showed a correlation between the amount of catalyst and the reduction of the integral of the acrylate peak of BDODA between 1658 and 1544 cm^{-1} (C=C stretching vibrations). The values were normalised to the constant CH-stretching vibrations between 3060 and 2770 cm^{-1}. FTIR spectra including a graph of the integral values are shown in figure 4.6.

However, when adding $AlCl_3$ powder to the reaction mixture, in some cases a harsh oxidation reaction took place, forming a brown, solid side product. Therefore, experiments using $AlCl_3$ as catalyst were stopped. Furthermore, decylamine was considered a better-suited reaction partner than Jeffamine® D 400; an amine of lower molar mass increased the reactivity and enhanced characterisation, as the basic structure was clearer.

So in the following series, a reaction between BDODA and decylamine with varying catalysts led to interesting results. For 4 different catalysis methods – (a) water at room temperature, (b) water, heated in an microwave oven, (c) $AlCl_3$ modified silica gel and (d) H_3BO_3 solution ($c_{H_3BO_3}$=0.3 mol/l) – the following reaction process was observed: Within some seconds of stirring, a white, wax-like substance precipitated in the inhomogeneous aqueous solution. For the microwave heated sample the shortest precipitation time was observed. The hydrophobic white substance had a melting temperature of about 40°C. Transmission FTIR as well as ^{1}H-NMR measurements in deuterated chloroform indicated a mono-addition of amine to the acrylate. ^{1}H-NMR spectra are shown in the appendix (figures 6.20 and 6.21). Exem-

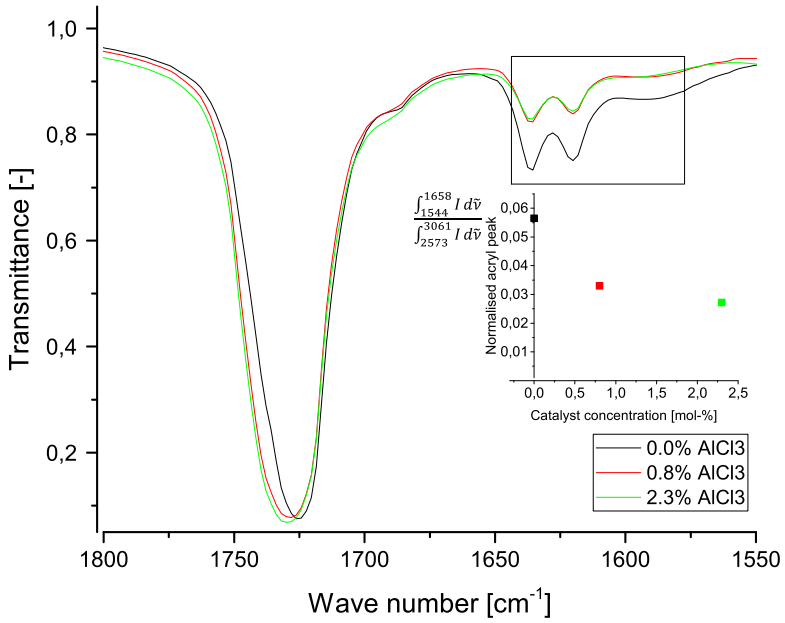

Figure 4.6: FTIR spectra of the reaction between BDODA and Jeffamine® D 400 for varying concentrations of $AlCl_3$ as catalyst

plary, the ^{1}H-NMR results of the reaction in water with microwave heating are listed and interpreted in table 4.3. The emphasised letters (**H$_2$**) therein designate the position of the hydrogen atoms of the given chemical shift.

For BDODA, characteristic ^{1}H-NMR peaks were expected at chemical shifts in the interval from 5.5-6.5 ppm. These disappeared completely, indicating the total conversion of the acrylate groups. Two reaction products were possible, firstly the mono-adduct (the reaction process is shown in figure 4.7) and secondly a bis-adduct (figure 4.8). According to the ^{1}H-NMR spectrum, both types were present with a high excess of the mono-adduct. Whilst the integral of methylene groups of the mono-adduct ranged close to total conversion (2 hydrogen atoms), the characteristic methyl groups of the bis-adduct led to integrals of approximately 0.05 hydrogen atoms. Therefore, the conversion grade to the bis-adduct accounted for 2.5 %. All integrals were referred to the integral of methyl peaks (3 hydrogen atoms) at the end of the aliphatic chain of decylamine. To conclude, the primary amine seemed to be preferred over the secondary amine for the aza-Michael reaction under these conditions.

The ^{1}H-NMR results were consistent with those of FTIR spectroscopy: Peaks for C=C stretching vibrations of acrylates were no longer present (see

Table 4.3: ^{1}H-NMR-shifts of characteristic groups in the reaction product of Michael reaction of BDODA and decylamine, catalysed with water and microwave heating

δ [ppm]	δ_{ref} [ppm]	Interpretation
equivalent to decylamine		
0.85 tr m	0.88	C**H$_3$**-(CH$_2$)$_9$-
1.24 brs s	1.29	C$_2$ in aliphatic chain
equivalent to acBDODA		
4.09 s s	4.13	-C(=O)OC**H$_2$**-
1.68 s s	1.62	-C(=O)OCH$_2$C**H$_2$**-
newly formed peaks - Monoaddition		
2.85 tr s	2.94	-NH-C**H$_2$**CH$_2$C=O-O-
2.58 tr s	2.55	-C**H$_2$**NH-
2.49 tr s	2.51	-NH-CH$_2$C**H$_2$**C=O-O-
1.45 tr s	1.38 or 1.44	-C**H$_2$**CH$_2$NH-; cyclohexane
newly formed peaks - Bisaddition		
3.66 tr w	3,76	-C**H$_2$**-N(C$_{10}$H$_{21}$)-C**H$_2$**-
3.19 tr w	3,01	R$_2$-N-C**H$_2$**-C$_9$H$_{19}$
further weak peaks		
3.44 tr, 2.74 tr, 2.66 tr, 2.41 m, 0.05 s		

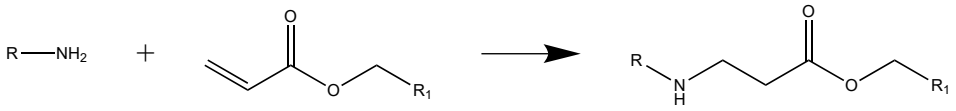

Figure 4.7: Formation of a mono-adduct via aza-Michael reaction

figure 6.22 in the appendix). For the sample catalysed with water at room temperature (RT), new peaks at 1650-1512 cm^{-1} appeared. No explanation for these peaks was found. Amide formation would shift the carbonyl peak and water would also lead to strong absorption bands in the region 3700-2700 cm^{-1}.

It was tried to perform FTIR reaction kinetics of the microwave-induced addition. However, the process was too fast: Total conversion took place within the first minute. No significant changes were observed between the product one minute or thirty minutes after the start of the reaction (see figure 6.23 in the appendix). Moreover, GCMS measurements were performed. The results did neither contradict the results of other methods, nor were they clear enough to add new findings. Figures 6.24 and 6.25 in the appendix show the GCMS graphs of educts and products.

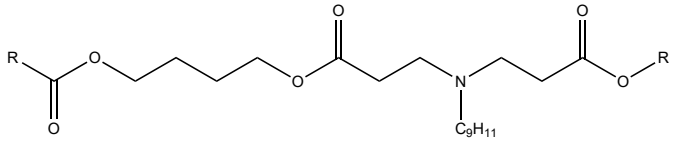

Figure 4.8: Side product of aza-Michael reaction of BDODA and decylamine, bis-adduct

CAN solution (c_{CAN}=0.3 mol/l) as a catalyst had a different effect. The reaction product was coloured due to the strong yellow colour of the catalyst. The product had a crumbly, rigid texture in the aqueous solution and was less homogeneous than the products described before. The ^{1}H-NMR spectrum (see figure 4.9) differed from those using the catalyst systems described before: Acrylate groups were still present and the most significant new peaks appeared at 3.31, 3.04 and 2.82 ppm. These results are neither consistent with secondary or tertiary amines obtained from Michael reaction, nor with products of radical polymerisation of the acrylate groups.

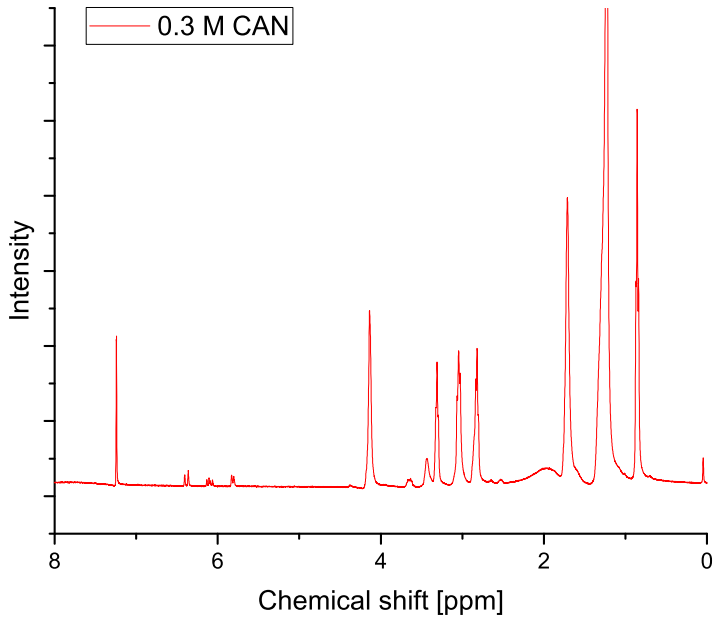

Figure 4.9: ^{1}H-NMR spectrum of the reaction mixture of BDODA and decylamine catalysed with CAN solution

To conclude, the following catalysis methods were proved successful for Michael reaction of BDODA and decylamine, whereby mono-adducts were

formed at high yields: $AlCl_3$-functionalised silica gel, water at room temperature, water heated with a microwave until the boiling point was reached and H_3BO_3 solution. The reaction sequence is shown in figure 4.7. A different reaction product was obtained for CAN solution, however, no interpretation for the product was found.

The results of the preliminary examination did not clarify which catalyst system was the best for Michael reaction of macromolecular acrylates. Therefore, in a secondary study, all catalyst systems were examined again for the reaction of PTHF1000ac and decylamine. The reaction proceeded more slowly. The product formed an inhomogeneous slurry in the aqueous reaction mixture instead of precipitation. In the FTIR spectra, at wave numbers from 1700-1600 cm^{-1}, a broad water peak obscured the area of C=C stretching vibrations in case of water as catalyst (see figure 6.26 (entire spectrum) and 6.27 (detailed view) in the appendix).

On the contrary, aqueous CAN-solution catalysed immediate reaction. The product which precipitated was not soluble in acetone, ethanol, chloroform, toluene or tetrahydrofurane. It was not possible to characterise the reaction neither by FTIR nor by ^{1}H-NMR.

Only for the series with microwave-induced reaction, the reaction progress could be monitored: Figure 4.10 shows the time-dependant change of the integral values in the region $\tilde{\nu}$=1658-1605 cm^{-1}. They are linked to C=C stretching vibrations. The values were normalised to constant CH stretching vibrations ($\tilde{\nu}$=3000-2770 cm^{-1}). Furthermore, a slight shift of the C=O stretching peak in acrylates from 1726 cm^{-1} to 1728 cm^{-1} was observed. The corresponding FTIR spectra are shown in figure 6.28 (entire spectrum) and figure 6.29 (detailed view) in the appendix.

To address the problem of characterisation, the microwave-induced reaction was performed in ethanol. PTHF1000ac and decylamine, as well as the reaction products, were soluble at any state of the reaction. Over the course of the reaction no change of properties such as viscosity or colour was perceived.

The ^{1}H-NMR spectra are shown in the appendix (figure 6.32). The following findings were derived: firstly, a significant reduction of the acrylate peaks. This is visualised in figure 4.11, the integrals were normalised to the integral of the hydrogen atoms characteristic for the ester group at δ= 4.16 ppm. This decrease of acrylate groups was also observed when analysing the reaction mixtures after 14 days, for microwave treatment, heating at 80 °C and at room temperature as well. The ^{1}H-NMR spectra of the reaction mixtures containing ethanol are shown in the appendix in figures 6.30 and 6.31.

The conversion of the acrylate group should proceed simultaneously with the formation of an aliphatic chain connecting the ester group and the amine. Despite intense efforts, total elucidation of the resulting structures was not achieved. Numerous new peaks appeared, which could be related to the

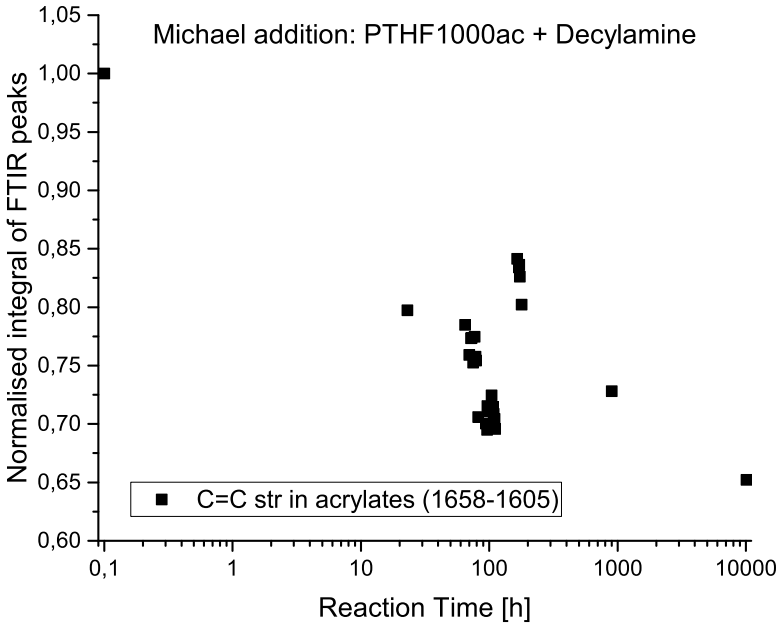

Figure 4.10: Time-dependant normalised integral values of FTIR spectra of the reaction mixture during microwave induced Michael reaction of PTHF1000 and decylamine

expected products, however, discrepancies in terms of the peaks' strength and stoichiometric values persisted. Nevertheless, it was possible to derive the following findings:

- Other reactions such as a oxo-Michael reaction or amine formation could be ruled out by the results of FTIR.
- For the mono- and the bis-adduct, ^{1}H-NMR-shifts of the protons of these methylene groups were expected according to values in figure 4.12. In both cases, peaks at a chemical shift of approximately δ=2.5 ppm were expected. This is substantiated by the results observed in the model reactions with BDODA.
- A weak peak at δ=2.67 ppm was already present in PTHF1000ac. Although it increased over the course of the reaction, it did not reflect the stoichiometry of the reduction of acrylate groups. For the mono-adduct, two peaks in this region were expected, which could not be found in sufficient intensity. For the bis-adduct, on the other hand, an evolution of peaks, which probably refer to its groups was observed (shown in figure 4.11)

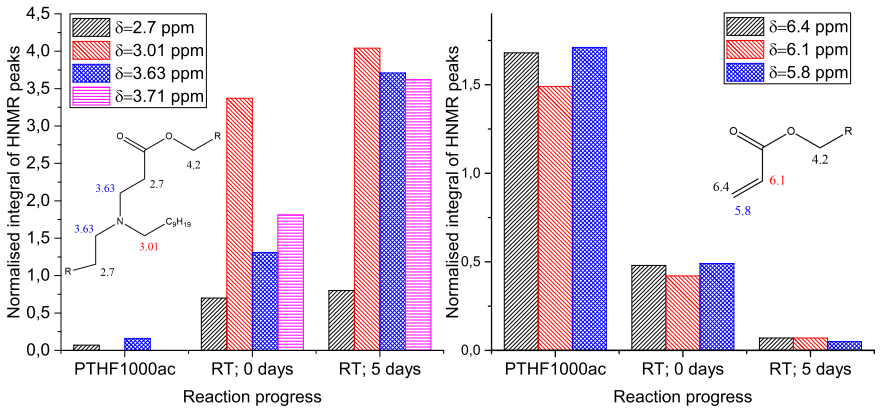

Figure 4.11: Development of the ^{1}H-NMR integral values at given chemical shifts δ, normalised to the hydrogen, bond to the ester group δ= 4.16 ppm

.

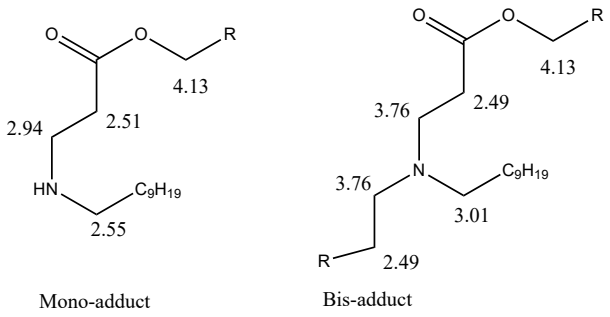

Figure 4.12: Chemical formula and ChemDraw ^{1}H-NMR predictions of aza-Michael reaction products.

To identify the product, a ^{13}C-NMR and a 2-dimensional NMR spectrum were recorded (see figure 6.33 and 6.34). Herein, apart from identification of the amine chain atoms, the ether and ester bonds, two newly formed peaks (1.3 ppm/14 ppm and 4.13 ppm/61.3 ppm) indicated the following: Both are characteristic of the methyl and the methylene group of a two carbon chain bond to an ether group (the chemical structure is illustrated in figure 4.13). Neither in ethanol nor in the desired end products such a group would appear. The most plausible explanation states that a trans-esterification of the polyol-acrylate with ethanol (solvent) had occurred.

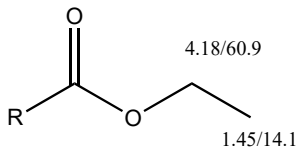

Figure 4.13: Chemical formula of the side product, obtained from transesterification of ethanol and PTHF1000ac (numbers indicate the measured ^{1}H-NMR and ^{13}C-NMR shifts)

4.4 Nanocomposites

The conditions derived from model reactions with PTHF1000ac and decylamine and the functionality of amine-modified silica nanoparticles examined in the second work package form a strong methodological basis for the further development of nano-composites. This development will be subject of a further study, as it would have exceeded the scope of this master thesis. Nevertheless, a first attempt to couple the acrylated polyols to the characterised nanoparticles was made.

Despite the risk of transesterification, the reaction was performed in ethanol, adding water as a catalyst. Under these conditions, no change of appearance was visually perceivable over the course of the reaction. To avoid agglomeration of the particles, no further drying step was performed before the ^{1}H-NMR measurements of the reaction mixture. Therefore, water as well as ethanol were still present. The spectra are shown in figure 4.14.

The most significant difference between the scan of the original reaction mixture and after five days with two intervals of microwave heating was the reduction of the integral of the acrylate groups. Unfortunately, a disturbance caused by water between 6.2 to 6.6 ppm made it impossible to evaluate the acrylate peaks at 6.4 and 6.1 ppm. Compared to the ester peak at 4.14 ppm, set to 3.51 ppm, the acrylate peak at 5.8 ppm was reduced from 1.94 ppm to 1.35 ppm, which equals a conversion of 30 %. At 3.28 ppm, a new peak formed for which no interpretation has yet been found.

To sum up, adding amine-modified silica nanoparticles to PTHF1000ac led to a conversion of acrylate groups. This is considered a positive first step for the on-going work on the formation of an elastomer.

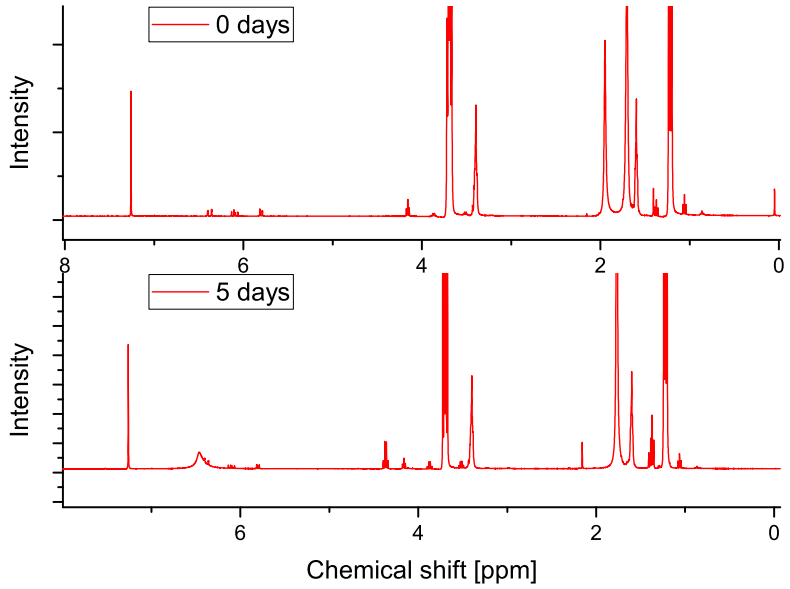

Figure 4.14: ^{1}H-NMR spectra of the reaction mixture of PTHF1000ac and amine-modified silica nanoparticles in ethanol for microwave-induced Michael reaction (water added) after 0 and 5 days reaction time

Chapter 5

Summary

Nanotechnology is a field of research which is attested the potential to fundamentally change various domains; amongst those, material sciences. Examples from nature strengthen the belief, that despite the technological difficulties which still persist, nano-structured materials will be a key to future technologies.

Polyurethanes used for vibration absorption, auto-assemble to nano-scaled structures. This results in their high potential for vibration attenuation. The idea behind the project this work is embedded in, is to form polyurethane-like elastomers. Instead of isocyanate and short-chained polyols, the hard segments should consist of silica nanoparticles; the soft segments remain equivalent to those in polyurethanes. Therefore the polyester-polyol PTHF was chosen as soft segment.

It is considered crucial, that the particles do not only act as a filler, but play the important role of crosslinking sites. To ensure this, a covalent binding is necessary. Before the properties of such a new material can be examined, the chemical foundations need to be laid. In this thesis, a potential method to form such covalent bonds between PTHF and silica nanoparticles was studied. Two main considerations led to the pursued strategy:

1. With regard to the applicability for the company partner, a process which does not necessitate particle modification was strongly desired. Tremendous efforts have already been taken to develop methods for the modification of nanoparticles. As a result, a range of modified particles is already commercially available. The most promising amongst those in terms of reactivity and costs are amine-modified silica nanoparticles.

2. In a next step, a convenient coupling mechanism between the primary amine and the polyol needed to be found. Amines react with a wide range of substances. The simple modification route via esterification with acrylic acid and the possibility to obtain dual-cure systems in a later stage, led to the decision to investigate the acrylation of polyols and their reactivity with amines.

The work is structured in three work packages:

1. The end group modification of polyetherols of different molar masses (PTHF250, PTHF1000, PTHF2000 and PTHF2900)

2. The characterisation of purchased amine modified silica nanoparticles

3. The determination of suited reaction conditions for aza-Michael reactions between acrylated polyols and model amine compounds

Finally, in a last experiment, the results of all steps were combined to couple the acrylated polyols to silica nanoparticles.

Hereafter, the methodology and the most important findings are recapped, the results are critically reviewed and in a final step and recommendations for further research are given:

In work package 1, the esterification reaction of PTHF with acrylic acid in cyclohexane was performed according to literature. The catalyst p-toluene sulphonic acid was added and hydroquinone was used as polymerisation inhibitor. The reaction was proven successful for 40 g polyol laboratory scale examples. Subsequently, the reaction also needed to be carried out for larger batches, firstly to obtain sufficient amounts of material for the following experiments and secondly to gather information about the up-scaling process. For high-molecular acrylated polyols, the purification procedure described in literature was insufficient and needed to be adapted. By addition of n-hexane to the quenched reaction mixture, the polarity of the organic phase was increased. Therefore, when purging with alkaline aqueous solution the product remained in the organic phase. The formation of an intermediate phase was reduced significantly. ^{1}H-NMR, ^{13}C-NMR and FTIR analysis showed conversion rates of 82-85% for PTHF1000ac and PTHF2000ac and of 80-100 % for PTHF2900ac. The thermal stability was investigated via TGA and pyrolysis GCMS. Compared to PTHF, the decomposition of acrylated PTHF shifted to higher temperatures. All results show that the acrylation was completed successfully.

In work package 2, commercially available amine-modified silica nanoparticles were characterised. Faced with insufficient supplier information, the nanoparticles functionality was determined in three different ways: TGA, titrations with HCl and p-TSA, and elemental analysis. The studied IoLiTec nanoparticles had a functionality of 2-2.5 mmol amine groups per gram of nanoparticles. Dynamic light scattering showed, that the hydrodynamic radius of the particles (20-200 nm) by far exceeded the range claimed in the supplier data sheet (10-20 nm).

Work package 3 comprised aza-Michael model reactions with BDODA and PTHF1000ac as Michael acceptors and decylamine as Michael donors. BDODA and decylamine reacted quickly, which was detectable via FTIR and ^{1}H-NMR spectroscopy. The high molar mass of PTHF1000ac slowed

down the reaction progress. Of all catalysts considered, an 1:1 mixture of the reactants with water and a heating step in a microwave oven led to the best results. For better characterisation, the same reaction was examined when dissolved in alcohol. Most probably in this case a bis-adduct was formed and trans-esterification took place as a side reaction.

In the experiment on aza-Michael reaction of nanoparticles and acrylated PTHF1000, a reduction of the characteristic ^{1}H-NMR peaks of acrylates was observed. However, despite the stoichiometric relations of the reactants, no elastomer-like cross-linked substance was produced.

To conclude, the findings show that aza-Michael reactions of long-chained acrylated PTHF is feasible, however, under the applied reaction conditions, it is not performing sufficiently. Another system with higher conversion rates at elevated reaction speed needs to be found.

The work evoked new questions, which should be further investigated. The experiments using CAN solution (c_{CAN}=1 mol/l) in ethanol as a catalyst produced an insoluble polymeric substance. Discovering the reaction mechanism could be of scientific and commercial interest.

On a long term, before commercialising nanoparticles-containing systems, their impact on health and safety needs to be monitored carefully.

Chapter 6

Appendix

Table 6.1: FTIR-shifts of characteristic groups in PTHF1000ac

ν_{region} cm^{-1}	ν_{peak} cm^{-1}	ν_{ref}[[64]] cm^{-1}	interpretation
newly formed peaks			
1750-1700	1726	1740-1705	C=O str in acrylates
1650-1625	1636	1640-1635	C=C str in acrylates
1625-1606	1620	1625-1620	C=C str in acrylates
1423-1339	1408	$\tilde{1}$410	$=CH_2$ δ
1329-1252	1259, 1270	1310-1250	C-O-C str in acrylates
1069-1046	1060	1070-1065	acrylate skeletal vibration
1020-911	983, 963	990-960	C=C δ in acrylates
850-780	810	810-800	$=CH_2$ twisting
peaks equivalent to PTHF1000			
3040-2715	2936, 2852, 2796	3000-2800	C-H str in CH_2
1500-1423	1450	1470-1435	$-CH_2-$ δ sym in esters
		1475-1460	$-CH_2-$ δ sym in ethers
		1480-1440	$-CH_2-$ δ
1162-1020	1100	1150-1060	C-O-C str in polyethers
780-711	746	845-765	C-O-C δ
711-682	666	695-645	C-O-C δ
1393-1329	1366	-	-
1252-1226	1241	-	-
1226-1162	1189	-	-

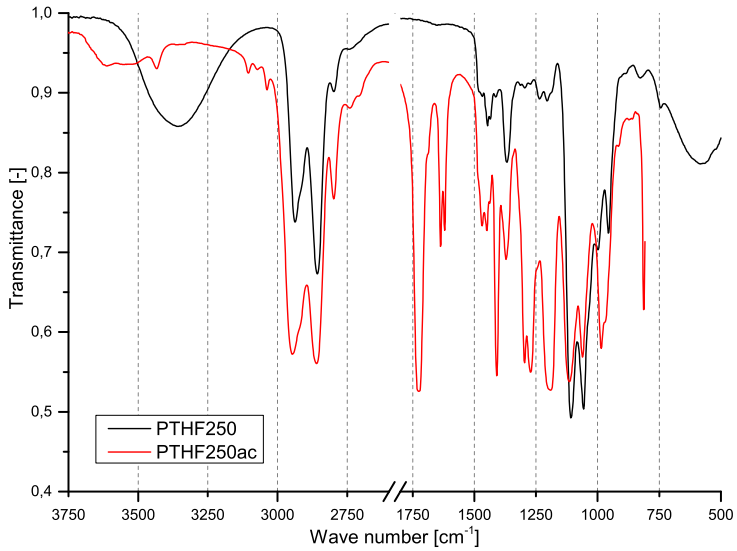

Figure 6.1: FTIR spectra of PTHF250 and PTHF250ac

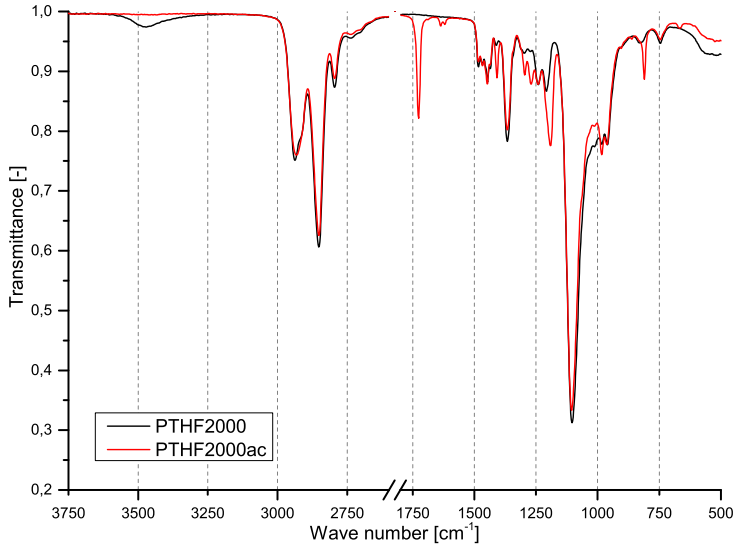

Figure 6.2: FTIR spectra of PTHF2000 and PTHF2000ac

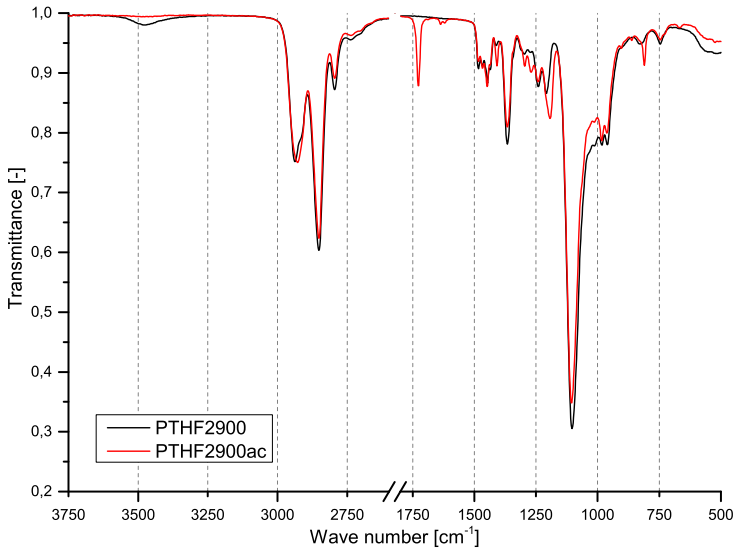

Figure 6.3: FTIR spectra of PTHF2900 and PTHF2900ac

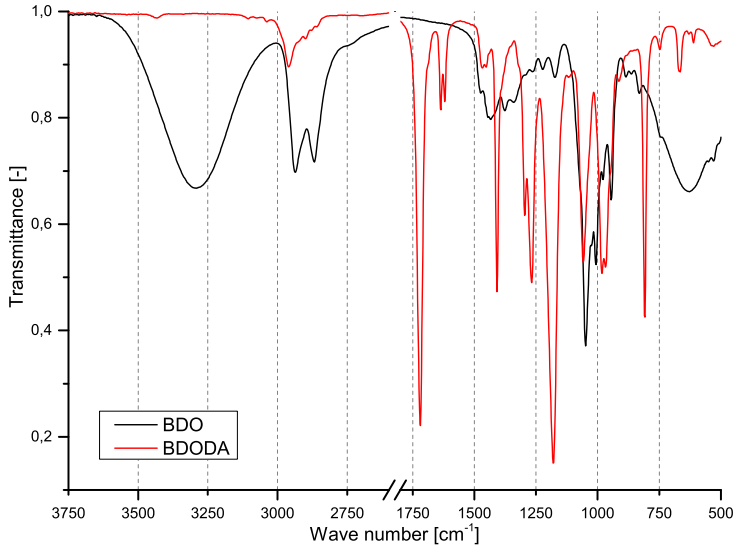

Figure 6.4: FTIR spectra of butanediol and BDODA

Table 6.2: ^{1}H-NMR shifts of characteristic groups of PTHF1000ac

δ [ppm]	δ_{ref} [ppm]	Interpretation	H	$H_{theoretical}$
equivalent to PTHF1000:				
3.61 tr	3.64[58]	-C**H$_2$**-OH	0.78	0
3.39 brs	3.40[16]	-O-C**H$_2$**-	50.4	50.4
1.60 brs	1.60[16]	-C**H$_2$**-	55.1	54.4
newly formed peaks:				
6.37 d	6.4 [16]	C**H$_2$**=CH-C(=O)-	1.68	2
6.09 q	6.18 [16]	CH$_2$=C**H**-C(=O)-	1.49	2
5.80 d	5.8 [16]	C**H$_2$**=CH-C(=O)-	1.71	2
4.16 tr	4.2 [16]	-C(=O)-O-C**H$_2$**-	3.51	4
further peaks:				
1.40 s	1.44 [58]	cyclohexane	2.82	
1.25 s			4.58	
0.86 tr	0.88 [58]	-CH$_3$	1.19	
weak peaks: 4.41 tr, 2.67 tr, 2.43 s, 2.02 s				

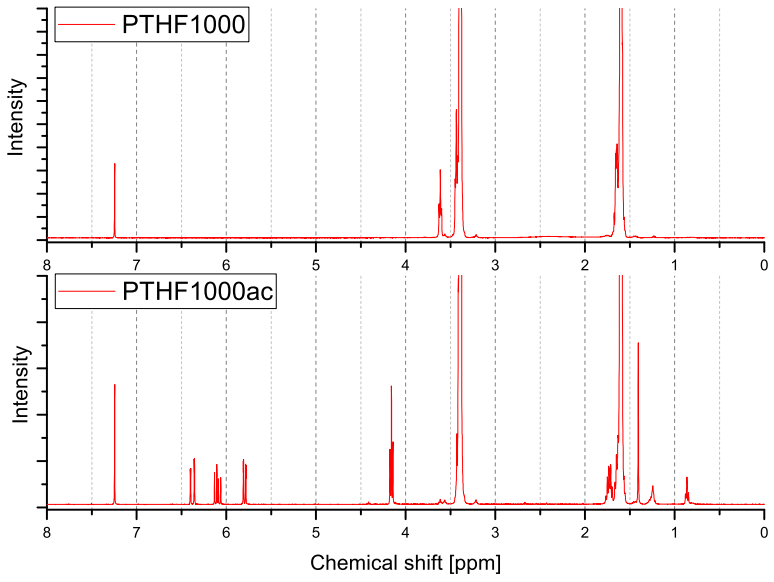

Figure 6.5: ^{1}H-NMR spectra of PTHF1000 and PTHF1000ac

Table 6.3: ^{1}H-NMR shifts of characteristic groups of PTHF2000ac

δ [ppm]	δ_{ref} [ppm]	Interpretation	H	$H_{theoretical}$
equivalent to PTHF2000:				
3.61 tr	3.64[58]	-C**H$_2$**-OH	0.19	0
3.39 brs	3.40[16]	-O-C**H$_2$**-	50.4	106
1.60 brs	1.60[16]	-C**H$_2$**-	53.8	112
newly formed peaks:				
6.37 d	6.4 [16]	C**H$_2$**=CH-C(=O)-	1.59	2
6.09 q	6.18 [16]	CH$_2$=C**H**-C(=O)-	1.45	2
5.80 d	5.8 [16]	C**H$_2$**=CH-C(=O)-	1.58	2
4.16 tr	4.2 [16]	-C(=O)-O-C**H$_2$**-	3.58	4
further peaks:				
1.41 s	1.44 [58]	cyclohexane	10.75	
1.25			1.65	
0.86 tr	0.88 [58]	-CH$_3$	1.16	
weak peaks: 4.41 tr, 2.67 tr, 2.43 s, 2.02 s, 1.25 s				

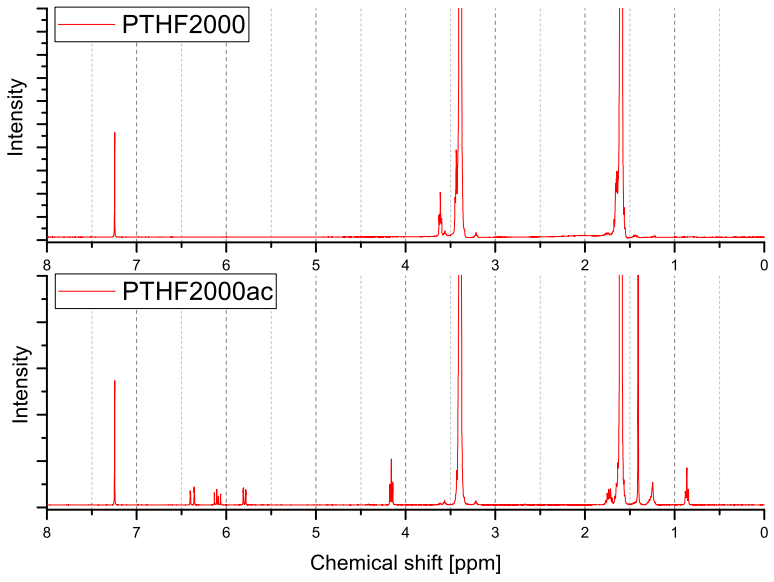

Figure 6.6: ^{1}H-NMR spectra of PTHF2000 and PTHF2000ac

Table 6.4: ^{1}H-NMR shifts of characteristic groups of PTHF2900ac

δ [ppm]	δ_{ref} [ppm]	Interpretation	H	$H_{theoretical}$
equivalent to PTHF2900:				
3.61 tr	3.64[58]	-CC**H$_2$**-OH	0.35	0
3.39 brs	3.40[16]	-O-CC**H$_2$**-	151.61	156
1.60 brs	1.60[16]	-CC**H$_2$**-	160	160
newly formed peaks:				
6.37 d	6.4 [16]	C**H$_2$**=CH-C(=O)-	1.83	2
6.09 q	6.18 [16]	CH$_2$=C**H**-C(=O)-	1.59	2
5.80 d	5.8 [16]	C**H$_2$**=CH-C(=O)-	1.96	2
4.16 tr	4.2 [16]	-C(=O)-O-C**H$_2$**-	4.03	4
further peaks:				
1.41 s	1.44 [58]	cyclohexane	18.19	
1.25			14.86	
0.86 tr	0.88 [58]	-CH$_3$	12.43	
weak peaks: 4.41 tr, 2.67 tr, 2.43 s				

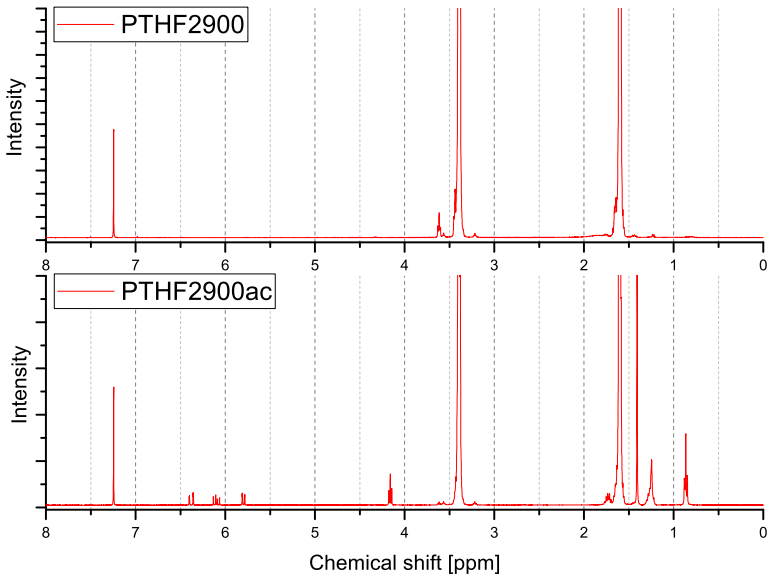

Figure 6.7: ^{1}H-NMR spectra of PTHF2900 and PTHF2900ac

Table 6.5: ^{13}C-NMR shifts of characteristic groups of PTHF1000, PTHF2000 and PTHF2900 including results of ChemDraw simulations δ_{ref}

δ *ppm*	δ_{ref} *ppm*	Interpretation
70.81; 70.58; 70.48	70.7	-**C**H_2-O-**C**H_2-
62.68	62.8	OH-**C**H_2-
30.35	29.2	OH-CH_2-**C**H_2
26.90; 26.48; 26.39	26.3	-O-CH_2-**C**H_2-

Table 6.6: ^{13}C-NMR shifts of characteristic groups of PTHF1000ac, PTHF2000ac and PTHF2900ac including results of ChemDraw simulations δ_{ref}

δ *ppm*	δ_{ref} *ppm*	Interpretation
equivalent to PTHF		
70.68; 70,59; 70.14	70.4	-**C**H_2-O-**C**H_2-
26.89; 26.48;26.24; 25.50	25.3	-O-CH_2-**C**H_2-
newly formed peaks		
166.25	166.5	CH_2=CH-**C**(=O)O-
130.49	131.3	**C**H_2=CH-C(=O)O-
128.53	128	CH_2=**C**H-C(=O)O-
64.38	65.3	CH_2=CH-C(=O)O**C**H_2-
impurities		
31.56	31.5	n-hexane, CH_3CH_2**C**H_2**C**$H_2CH_2CH_3$
22.63	22.7	n-hexane, CH_3**C**$H_2CH_2CH_2$**C**H_2CH_3
14.10	14.1	n-hexane **C**$H_3CH_2CH_2CH_2CH_2$**C**H_3

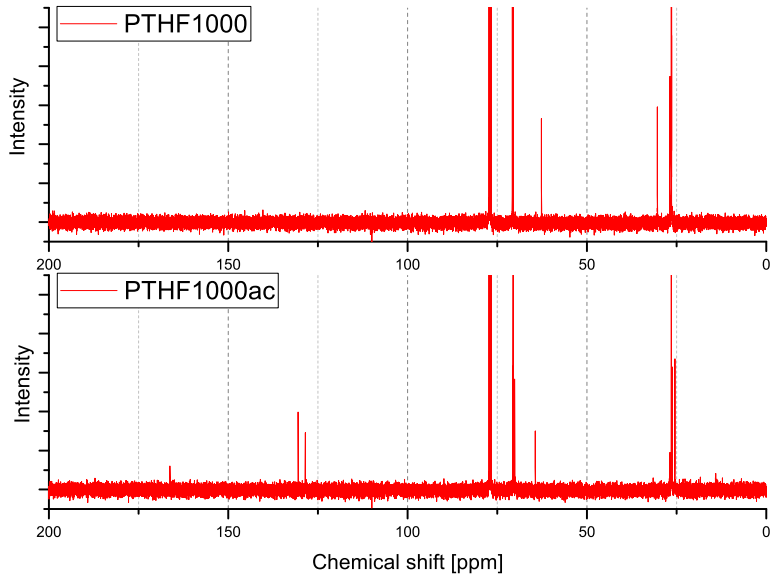

Figure 6.8: ^{13}C-NMR spectra of PTHF1000 and PTHF1000ac

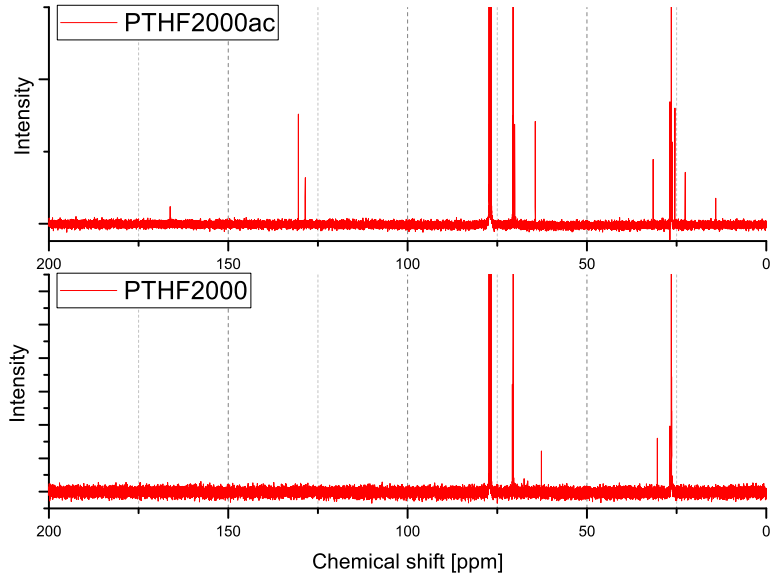

Figure 6.9: ^{13}C-NMR spectra of PTHF2000 and PTHF2000ac

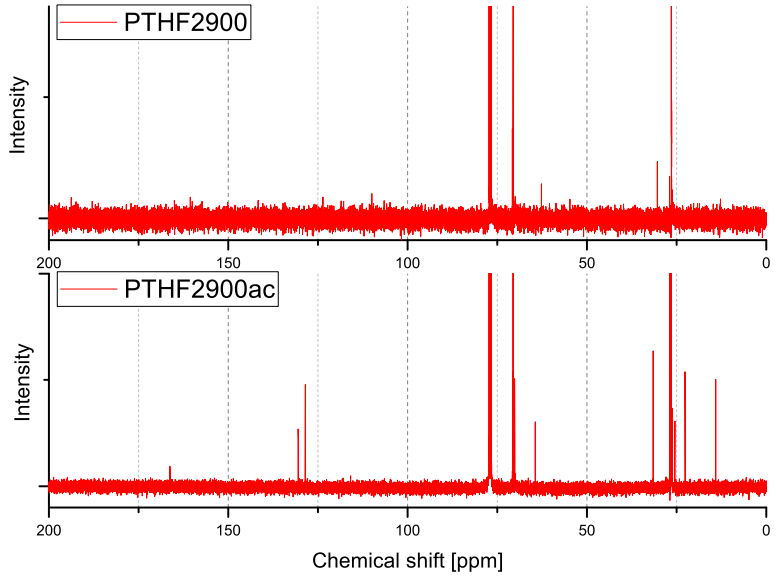

Figure 6.10: ^{13}C-NMR spectra of PTHF2900 and PTHF2900ac

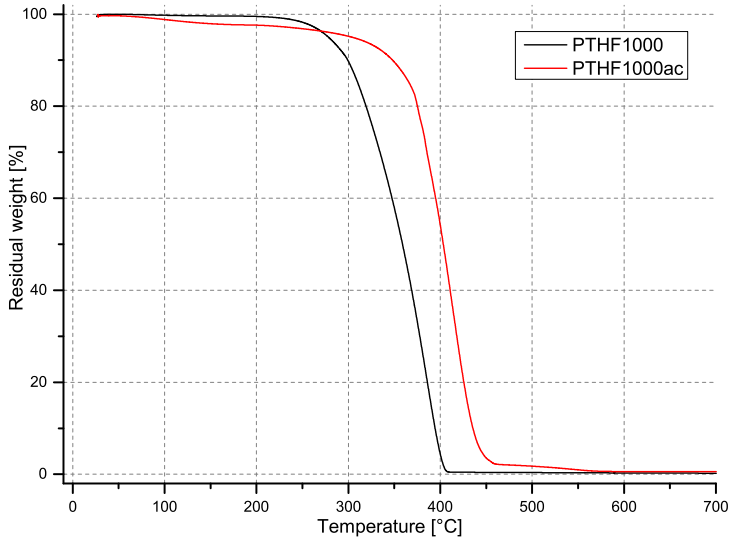

Figure 6.11: TGA of PTHF1000 and PTHF1000ac

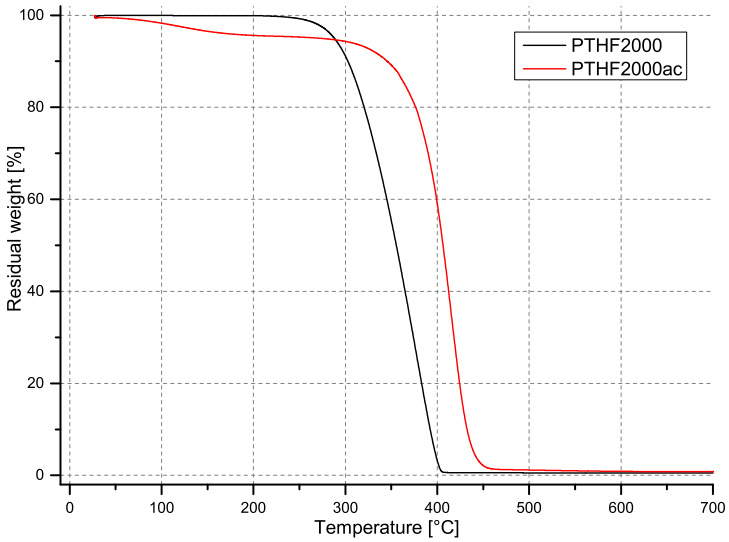

Figure 6.12: TGA of PTHF2000 and PTHF2000ac

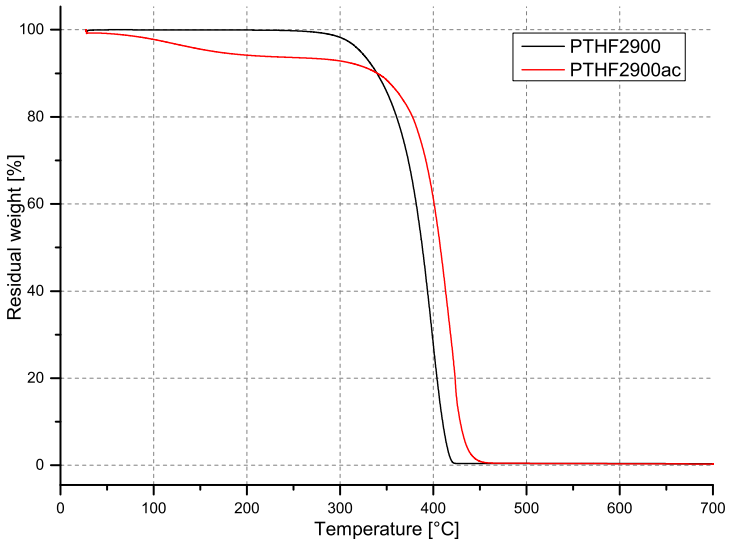

Figure 6.13: TGA of PTHF2900 and PTHF2900ac

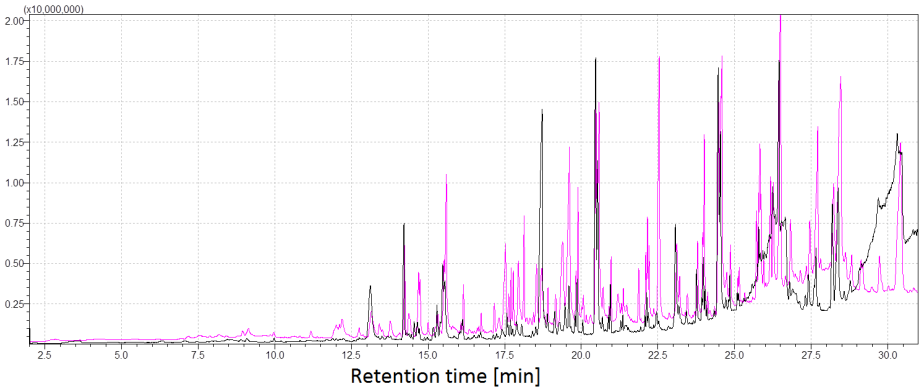

Figure 6.14: Pyrolysis GCMS of PTHF2000 (black) and PTHF2000ac (pink) at 200 °C

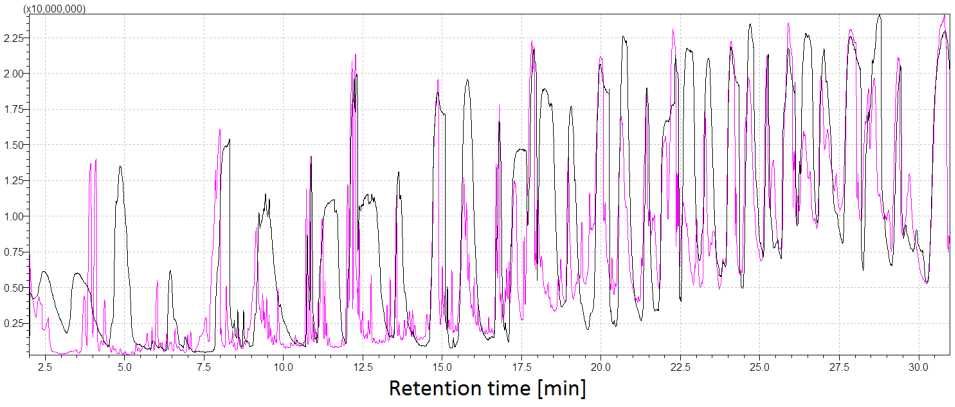

Figure 6.15: Pyrolysis GCMS of PTHF2000 (black) and PTHF2000ac (pink) at 600 °C

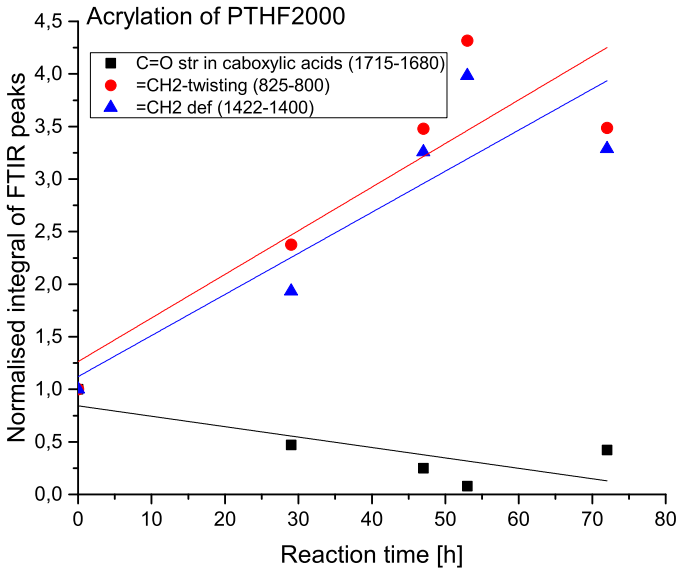

Figure 6.16: Graph of time-dependant normalised integral values of FTIR spectra of the reaction mixture during acrylation of PTHF2000

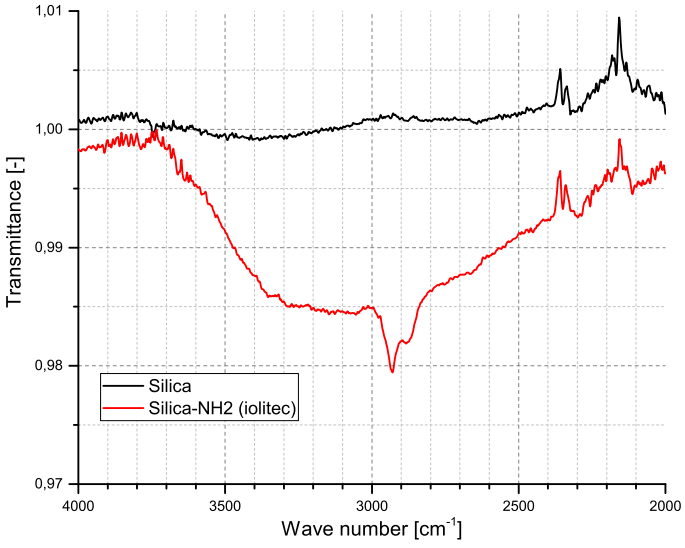

Figure 6.17: FTIR spectrum ($\tilde{\nu}$=4000-2000 cm^{-1}) of amine-modified silica nanoparticles and non-modified silica

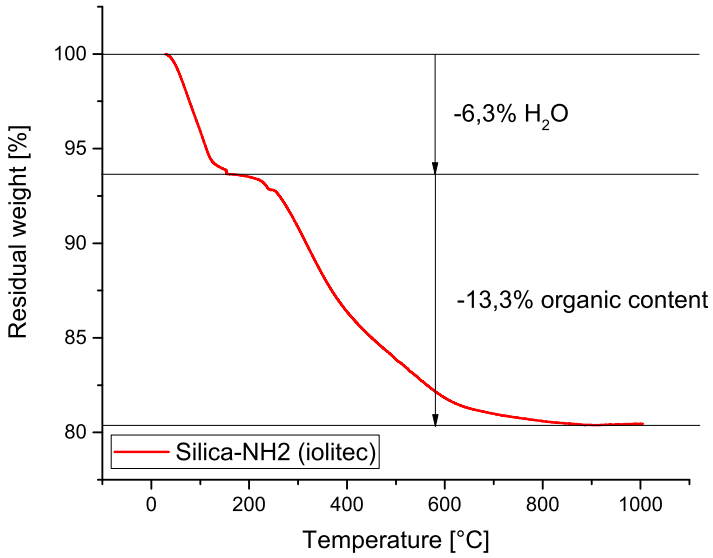

Figure 6.18: TGA of amine-modified silica nanoparticles

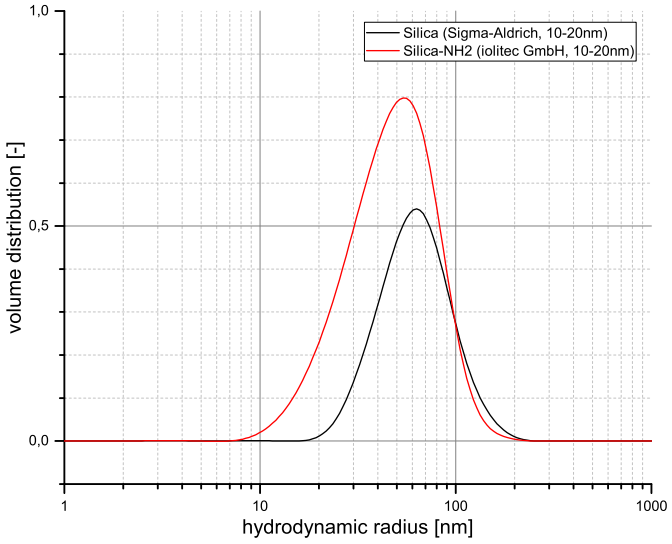

Figure 6.19: Volume distribution of the hydrodynamic radius of SiO_2–NP+NH_2 and non-modified nanoparticles measured via DLS

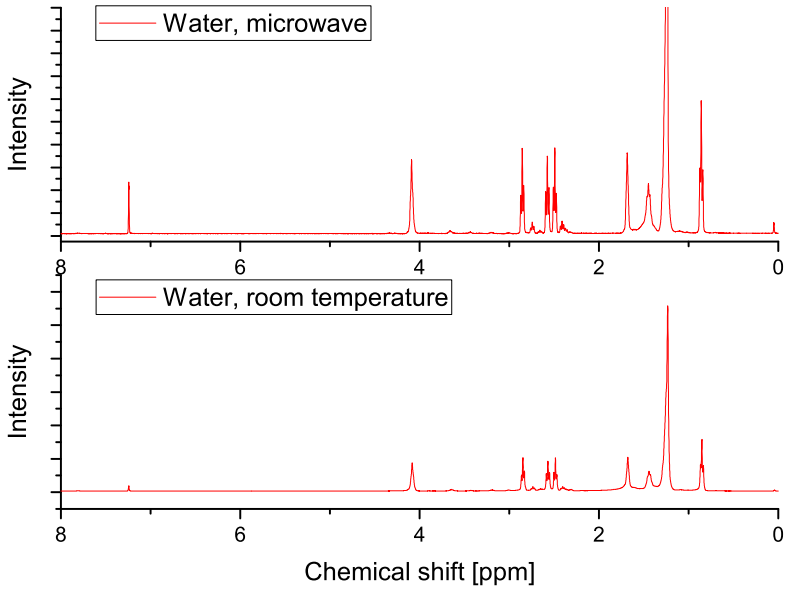

Figure 6.20: ^{1}H-NMR spectra of the reaction mixture of BDODA and decylamine catalysed with water, microwave-heated and at room temperature

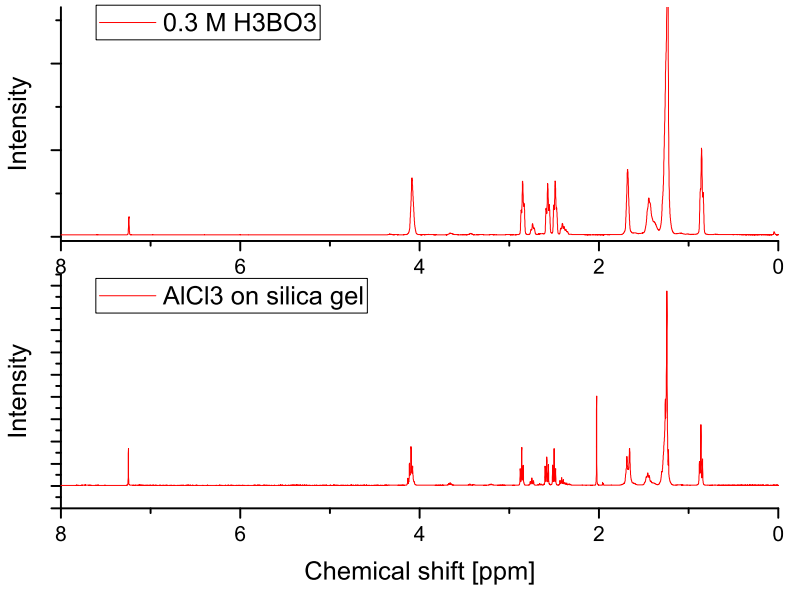

Figure 6.21: ^{1}H-NMR spectra of the reaction mixture of BDODA and decylamine catalysed with H_3BO_3 solution and $AlCl_3$ on silica gel

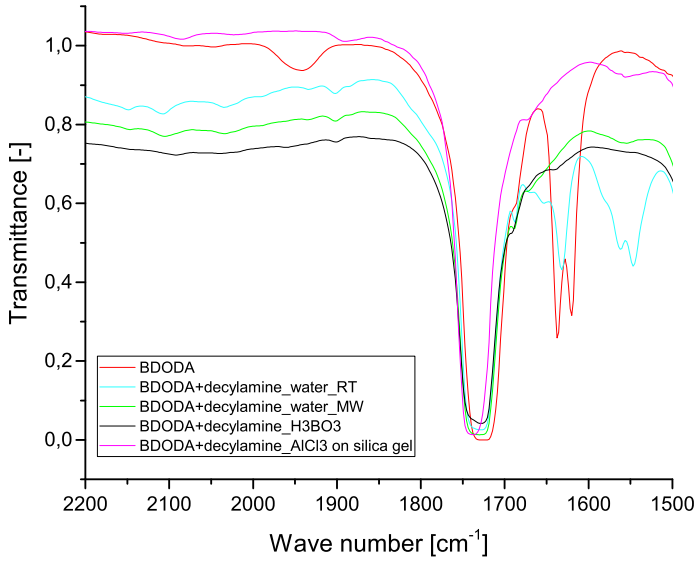

Figure 6.22: FTIR spectra ($\tilde{\nu}$=1500-2000 cm^{-1}) of the reaction mixture of BDODA and decylamine with varying catalysts

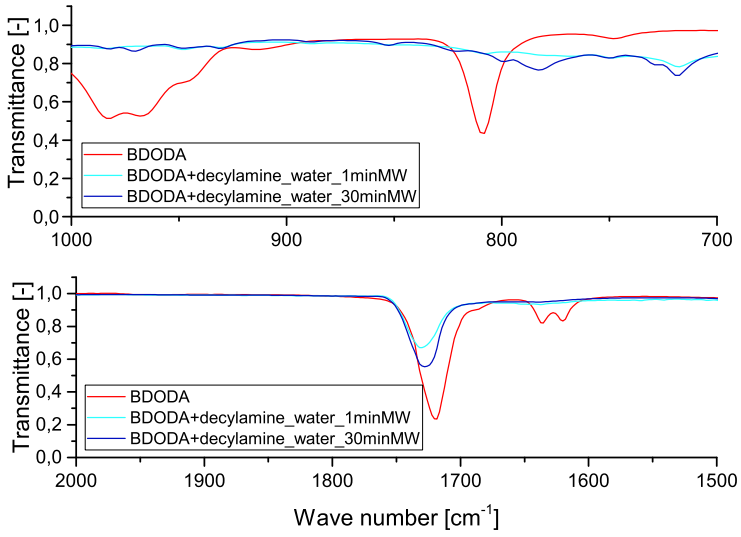

Figure 6.23: Time-dependant FTIR spectra ($\tilde{\nu}$=200-500 cm^{-1}; 1000-500 cm^{-1}) of the reaction mixture of BDODA and decylamine for microwave-induced Michael reaction in water

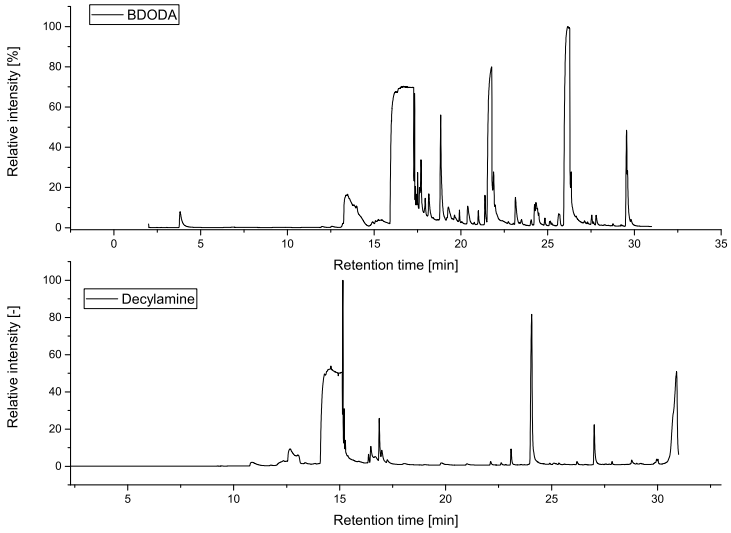

Figure 6.24: GCMS of BDODA and decylamine

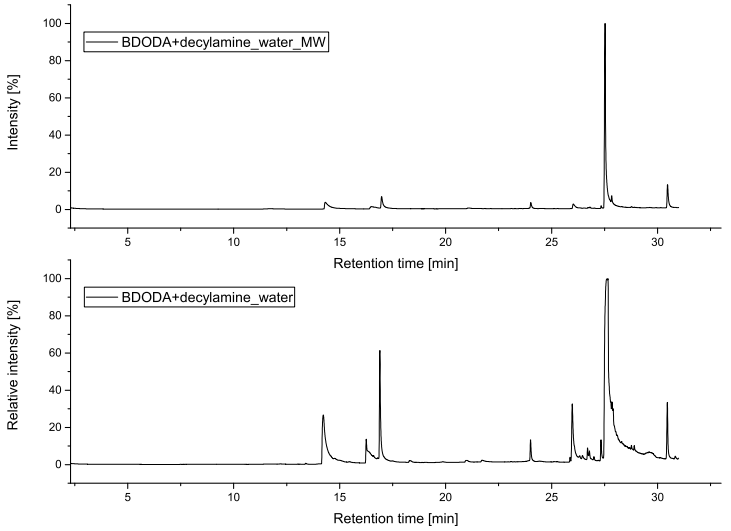

Figure 6.25: GCMS of the reaction mixture of BDODA and decylamine catalysed with water at room temperature and under microwave-heating

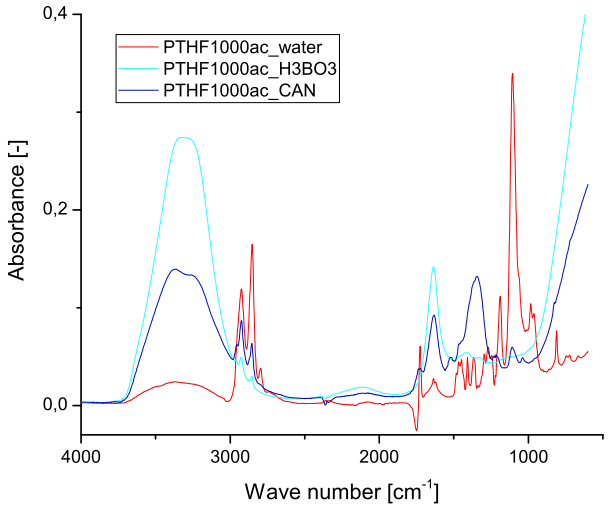

Figure 6.26: FTIR spectra of the reaction mixture of PTHF1000ac and decylamine for varying catalysts in aqueous solutions

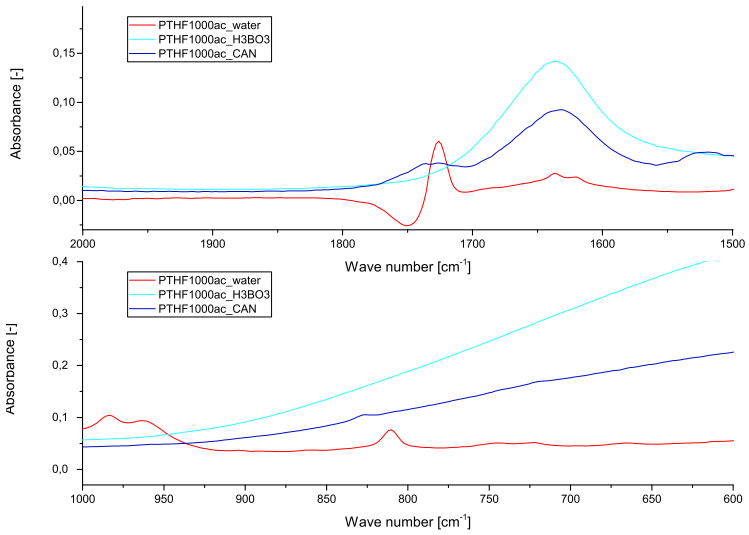

Figure 6.27: Detailed view of FTIR spectra of the reaction mixture of PTHF1000ac and decylamine for varying catalysts in aqueous solutions ($\tilde{\nu}$=2000-1500 cm^{-1}; 1000-600 cm^{-1})

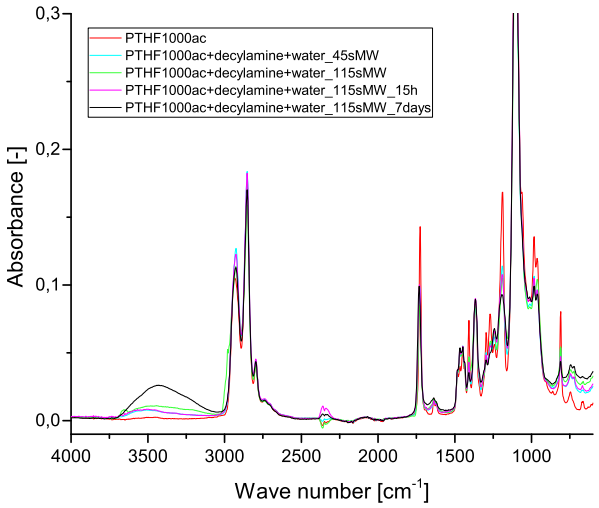

Figure 6.28: Time-dependant FTIR spectra of the reaction mixture of PTHF1000ac and decylamine for microwave-induced Michael reaction in water

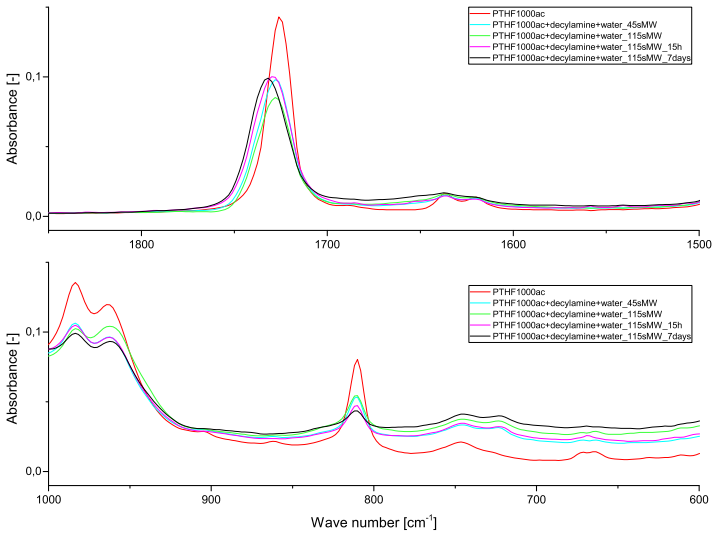

Figure 6.29: Detailed view of time-dependant FTIR spectra of the reaction mixture of PTHF1000ac and decylamine for microwave-induced Michael reaction in water ($\tilde{\nu}$=2000-1500 cm^{-1}; 1000-600 cm^{-1})

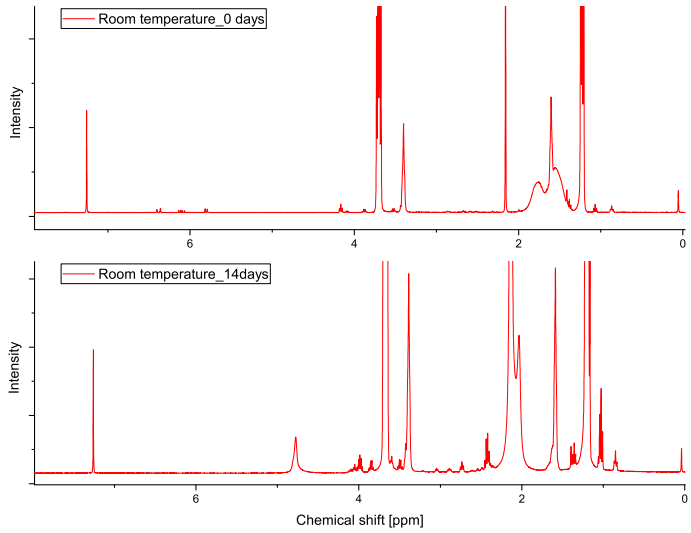

Figure 6.30: ^{1}H-NMR spectra of the reaction mixture of PTHF1000ac and decylamine in ethanol after 0 and 14 days reaction time

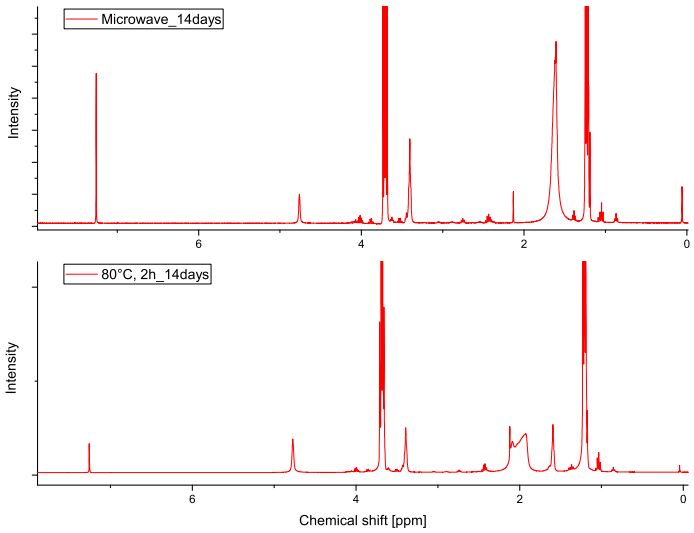

Figure 6.31: ^{1}H-NMR spectra of the reaction mixture of PTHF1000ac and decylamine in ethanol with 15 s microwave treatment or 2 h reflux heating at 80 °C after 14 days reaction time

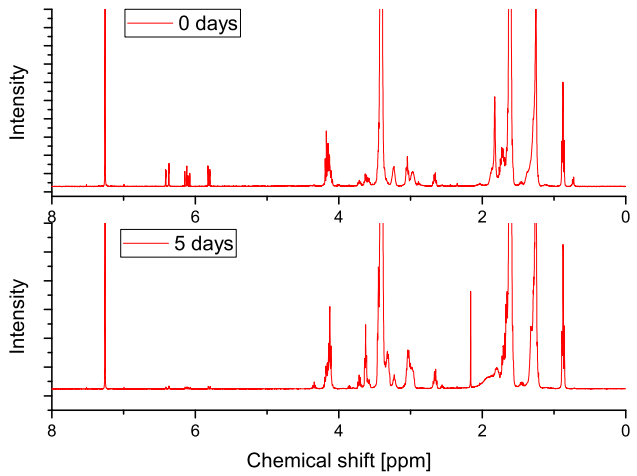

Figure 6.32: ^{1}H-NMR spectra of the centrifuged reaction mixture of PTHF1000ac and decylamine in ethanol for microwave-induced Michael reaction (water added) after 0 and 5 days reaction time

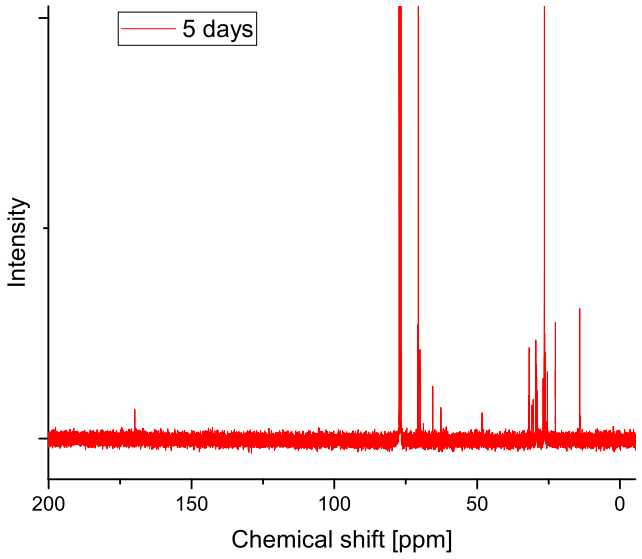

Figure 6.33: ^{13}C-NMR spectrum of the centrifuged reaction mixture of PTHF1000ac and decylamine in ethanol for microwave-induced Michael reaction (water added) after 5 days reaction time

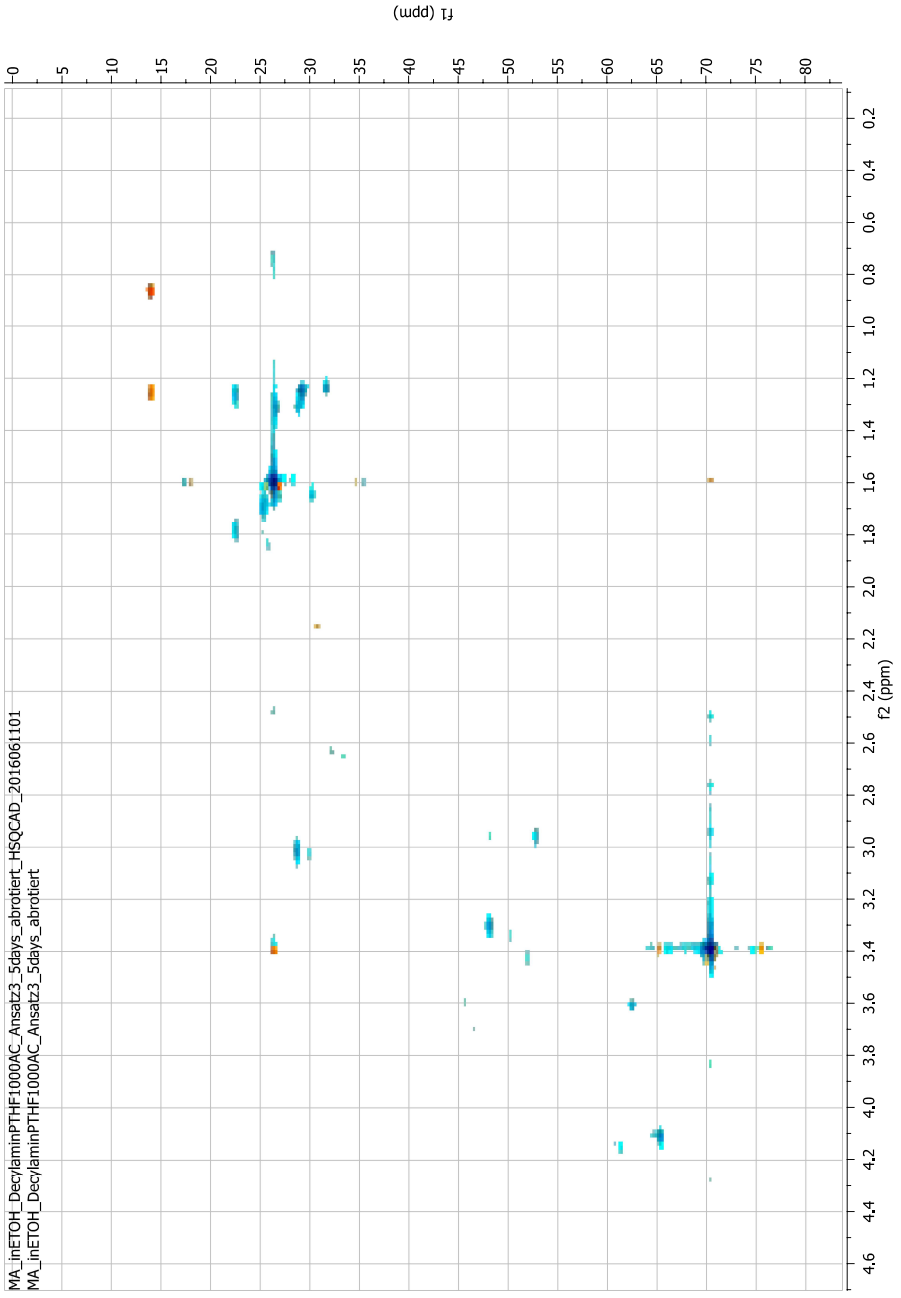

Figure 6.34: 2-dimensional NMR spectrum of the centrifuged reaction mixture of PTHF1000ac and decylamine in ethanol for microwave-induced Michael reaction (water added) after 5 days reaction time

Bibliography

[1] C. Prisacariu. *Polyurethane elastomers: From morphology to mechanical aspects*. Wien and New York: Springer, 2011. ISBN: 978-3-7091-0514-6.

[2] J.A. Koutsky, N.V. Hien, and S.L. Cooper. "Some results on electron microscope investigations of polyether-urethane and polyester-urethane block copolymers". In: *Journal of Polymer Science Part B: Polymer Letters* 8.5 (1970), pp. 353–359.

[3] N.S. Schneider et al. "Structural studies of crystalline MDI-based polyurethanes". In: *Journal of Macromolecular Science, Part B: Physics* 11.4 (1975), pp. 527–552.

[4] Environmental Protection Agency (EPA) US Environment Protection Agency. *Significant New Use Rules: Toluene Diisocyanates and Related Compounds*. 15.01.2015. URL: `https://www.regulations.gov/document?D=EPA-HQ-OPPT-2011-0976-0001`.

[5] D.C. Allport, D. S. Gilbert, and S. M. Outterside. *MDI and TDI: A safety, health and the environment : a source book and practical guide*. New York: J. Wiley, 2003. ISBN: 978-0-471-95812-3.

[6] I.L. Bernstein. "Isocyanate-induced pulmonary diseases: a current perspective". In: *Journal of Allergy and Clinical Immunology* 70.1 (1982), pp. 24–31.

[7] G. Rokicki, Paweł G. Parzuchowski, and M. Mazurek. "Non-isocyanate polyurethanes: synthesis, properties, and applications". In: *Polymers for Advanced Technologies* 26.7 (2015), pp. 707–761.

[8] O. Figovsky et al. "Recent advances in the development of non-isocyanate polyurethanes based on cyclic carbonates". In: *PU MAGAZINE, 2013, 10, 4, 256* 263 (2013).

[9] O. Figovsky. *Green Polyurethane*. Ed. by Nano Tech Industries. 2016. URL: `http://www.nanotechindustriesinc.com/GPU.php`.

[10] O. Birukov et al. *Nanostructured hybrid oligomer composition*. US Patent 7,820,779. Oct. 2010. URL: `https://www.google.com/patents/US7820779`.

[11] O. Figovsky, D. Beilin, and N. Blank. "Advanced Material Nanotechnology in Israel". In: *Nanomaterials: Risks and Benefits*. Ed. by Igor Linkov. NATO Science for Peace and Security Series C, Environmental Security. Dordrecht: Springer Netherlands, 2009, pp. 275–286. ISBN: 978-1-4020-9491-0.

[12] O. Türünç et al. "Nonisocyanate based polyurethane/silica nanocomposites and their coating performance". In: *Journal of Sol-Gel Science and Technology* 47.3 (2008), pp. 290–299.

[13] A.K. Gaharwar et al. "Transparent, elastomeric and tough hydrogels from poly (ethylene glycol) and silicate nanoparticles". In: *Acta biomaterialia* 7.12 (2011), pp. 4139–4148.

[14] Y. Guan et al. "Polytetrahydrofuran amphiphilic networks. I. Synthesis and characterization of polytetrahydrofuran acrylate ditelechelic and polyacrylamide-l-polytetrahydrofuran networks". In: *Journal of Polymer Science Part A: Polymer Chemistry* 38.20 (2000), pp. 3812–3820.

[15] G. Malucelli et al. "Photopolymerization of poly (tetramethylene ether) glycol diacrylates and properties of the obtained networks". In: *Polymer* 37.12 (1996), pp. 2565–2571.

[16] W. Meyer et al. "Soft polymers for building up small and smallest blood supplying systems by stereolithography". In: *Journal of functional biomaterials* 3.2 (2012), pp. 257–268.

[17] A.Y. Rulev. "Aza-Michael reaction: Achievements and prospects". English. In: *Russian Chemical Reviews* 80.3 (2011), pp. 197–218.

[18] H. Hart and N. Kindler. *Organische Chemie*. 3., vollst. überarb. und aktualisierte Aufl. Bachelor. Weinheim: Wiley-VCH, 2007. ISBN: 978-3-527-31801-8.

[19] K.P.C. Vollhardt and N.E. Schore. *Organische Chemie: Set aus Lehrbuch und Arbeitsbuch*. 5., Auflage. Weinheim: Wiley-VCH, 2012, 912ff, 1126. ISBN: 978-3-527-32754-6.

[20] D.P. Nair et al. "The thiol-Michael addition click reaction: a powerful and widely used tool in materials chemistry". In: *Chemistry of Materials* 26.1 (2013), pp. 724–744.

[21] O.A. Neumüller. *A - Cl*. 8., neubearb. und erw. Aufl., 51. - 61. Tsd. Vol. / Otto-Albrecht Neumüller ; Bd. 1. Römpps Chemie-Lexikon. Stuttgart: Franckh, 1979. ISBN: 3-440-04511-0.

[22] H.G.O. Becker. *Organikum: Organisch-chemisches Grundpraktikum ; mit 220 Tabellen und einem Faltblatt*. 20., bearb. und erw. Aufl. Heidelberg [u.a.]: Barth, 1996. ISBN: 3-335-00492-2.

[23] M. Sibi and S. Manyem. "Enantioselective Conjugate Additions". English. In: *Tetrahedron* 56.41 (2000), pp. 8033–8061.

[24] M. Liu and M.P. Sibi. "Recent advances in the stereoselective synthesis of β-amino acids". English. In: *Tetrahedron* 58.40 (2002), pp. 7991–8035.

[25] B.D. Mather et al. "Michael addition reactions in macromolecular design for emerging technologies". English. In: *Progress in Polymer Science* 31.5 (2006), pp. 487–531.

[26] D. Rosenthal et al. "The Synthesis of β-Amino Mercaptans and β-Amino Thiosulfates via Ethylenimine Intermediates1". In: *The Journal of Organic Chemistry* 30.11 (1965), pp. 3689–3696.

[27] M.K. Chaudhuri et al. "Boric acid: a novel and safe catalyst for aza-Michael reactions in water". In: *Tetrahedron letters* 46.48 (2005), pp. 8329–8331.

[28] M.R. Saidi, Y. Pourshojaei, and F. Aryanasab. "Highly Efficient Michael Addition Reaction of Amines Catalyzed by Silica-Supported Aluminum Chloride". In: *Synthetic Communications* 39.6 (2009), pp. 1109–1119. ISSN: 0039-7911. DOI: 10.1080/00397910802499559.

[29] R. Varala, N. Sreelatha, and S. R. Adapa. "Ceric ammonium nitrate catalyzed aza-Michael addition of aliphatic amines to α, β-unsaturated carbonyl compounds and nitriles in water". In: *Synlett* 2006.10 (2006), pp. 1549–1553.

[30] M. Pagliaro. *Nano-age: How nanotechnology changes our future*. Weinheim: Wiley-VCH, 2010. ISBN: 978-3-527-32676-1.

[31] D. Vollath. *Nanoparticles-nancomposites-nanomaterials*. Weinheim: Wiley-VCH, 2013. ISBN: 978-3-527-33460-5.

[32] H. Gao et al. "Materials become insensitive to flaws at nanoscale: Lessons from nature". In: *Proceedings of the National Academy of Sciences* 100.10 (2003), pp. 5597–5600. eprint: http://www.pnas.org/content/100/10/5597.full.pdf. URL: http://www.pnas.org/content/100/10/5597.abstract.

[33] A. Cho. "Connecting the dots to custom catalysts". In: *Science (New York, N.Y.)* 299.5613 (2003), pp. 1684–1685. ISSN: 0036-8075. DOI: 10.1126/science.299.5613.1684.

[34] M.M.B. Holl. "Nanotoxicology: a personal perspective". In: *Wiley Interdisciplinary Reviews: Nanomedicine and Nanobiotechnology* 1.4 (2009), pp. 353–359. ISSN: 1939-0041. DOI: 10.1002/wnan.27. URL: http://dx.doi.org/10.1002/wnan.27.

[35] L. Yildirimer et al. "Toxicology and clinical potential of nanoparticles". In: *Nano Today* 6.6 (2011), pp. 585–607. ISSN: 1748-0132. DOI: http://dx.doi.org/10.1016/j.nantod.2011.10.001. URL: http://www.sciencedirect.com/science/article/pii/S1748013211001137.

[36] J. Jordan et al. "Experimental trends in polymer nanocomposites - a review". In: *Materials science and engineering: A* 393.1 (2005), pp. 1–11.

[37] W. Kaiser. *Kunststoffchemie für Ingenieure: Von der Synthese bis zur Anwendung*. 4., neu bearbeitete und erweiterte Auflage. München: Hanser, 2016, pp. 100–101. ISBN: 978-3-446-44638-0.

[38] G. Menges. *Werkstoffkunde Kunststoffe*. 6., vollständig überarbeitete Auflage. München: Hanser, Carl, 2011. ISBN: 978-3-446-42762-4.

[39] S. Kango et al. "Surface modification of inorganic nanoparticles for development of organic-inorganic nanocomposites - A review". In: *Progress in Polymer Science* 38.8 (2013). Topical Issue on Polymer Hybrids, pp. 1232–1261. ISSN: 0079-6700. DOI: http://dx.doi.org/10.1016/j.progpolymsci.2013.02.003. URL: http://www.sciencedirect.com/science/article/pii/S0079670013000105.

[40] H. Briehl. *Chemie der Werkstoffe*. 3., überarb. u. erw. Aufl. 2014. SpringerLink : Bücher. Wiesbaden: Springer Vieweg, 2014, pp. 54–56. ISBN: 978-3-658-06225-5.

[41] *Ullmann's Encyclopedia of Industrial Chemistry*. Weinheim, Germany: Wiley-VCH Verlag GmbH & Co. KGaA, 2000. ISBN: 3527306730. DOI: 10.1002/14356007.

[42] K. Friedrich, S. Fakirov, and Z. Zhang. *Polymer composites: From nano-to-macro-scale*. New York: Springer, 2005, pp. 63–103. ISBN: 978-0387-24176-0.

[43] S. Varghese et al. "Morphology and mechanical properties of layered silicate reinforced natural and polyurethane rubber blends produced by latex compounding". In: *Journal of applied polymer science* 92.1 (2004), pp. 543–551.

[44] "Amorphe Kieselsäure. MAK Value Documentation in German language, 1989". In: *The MAK-Collection for Occupational Health and Safety*. Weinheim, Germany: Wiley-VCH Verlag GmbH & Co. KGaA, 2012, pp. 1–26. ISBN: 3527600418.

[45] G. Wang, L. Zhang, and G. He. *Prepn. for controllable grain size non-crystal nm silicon dioxide*. CN Patent 1,046,921. Dec. 1999. URL: https://www.google.at/patents/CN1046921C?cl=en.

[46] C.L. Wu et al. "Silica nanoparticles filled polypropylene: effects of particle surface treatment, matrix ductility and particle species on mechanical performance of the composites". In: *Composites Science and Technology* 65.3 – 4 (2005). JNC13-AMAC-Strasbourg, pp. 635–645. ISSN: 0266-3538. DOI: http://dx.doi.org/10.1016/j.compscitech.2004.09.004. URL: http://www.sciencedirect.com/science/article/pii/S0266353804002064.

[47] W. Stöber, A. Fink, and E. Bohn. "Controlled growth of monodisperse silica spheres in the micron size range". In: *Journal of colloid and interface science* 26.1 (1968), pp. 62–69.

[48] A. Liberman et al. "Synthesis and surface functionalization of silica nanoparticles for nanomedicine". In: *Surface science reports* 69.2 (2014), pp. 132–158.

[49] X. Song et al. "Chemical mechanical polishing removal rate and mechanism of semiconductor silicon with nano-SiO_2 slurries". In: *Journal of the Chinese Ceramic Society* 8 (2008), p. 034.

[50] K. Aschberger et al. "Nanomaterials in Food-Current and Future Applications and Regulatory Aspects". In: *Journal of Physics: Conference Series*. Vol. 617. 1. IOP Publishing. 2015, p. 012032.

[51] M.A. Albrecht, C.W. Evans, and C.L. Raston. "Green chemistry and the health implications of nanoparticles". In: *Green Chemistry* 8.5 (2006), pp. 417–432.

[52] R.P. Bagwe, L.R. Hilliard, and W. Tan. "Surface modification of silica nanoparticles to reduce aggregation and nonspecific binding". In: *Langmuir* 22.9 (2006), pp. 4357–4362.

[53] M. Pagliaro. "Chapter 1 Functionalized Silicas: the Principles". In: *Silica-Based Materials for Advanced Chemical Applications*. The Royal Society of Chemistry, 2009, pp. 1–38. ISBN: 978-1-84755-898-5. DOI: 10.1039/9781847557162-00001. URL: http://dx.doi.org/10.1039/9781847557162-00001.

[54] H.T. Lu. "Synthesis and characterization of amino-functionalized silica nanoparticles". In: *Colloid Journal* 75.3 (2013), pp. 311–318.

[55] W.C. Bigelow, D.L. Pickett, and W.A. Zisman. "Oleophobic monolayers". In: *Journal of Colloid Science* 1.6 (1946), pp. 513–538. ISSN: 0095-8522. DOI: http://dx.doi.org/10.1016/0095-8522(46)90059-1. URL: http://www.sciencedirect.com/science/article/pii/0095852246900591.

[56] I.A. Rahman, M. Jafarzadeh, and C.S. Sipaut. "Synthesis of organo-functionalized nanosilica via a co-condensation modification using γ-aminopropyltriethoxysilane (APTES)". In: *Ceramics International* 35.5 (2009), pp. 1883–1888. ISSN: 0272-8842. DOI: http://dx.doi.org/10.1016/j.ceramint.2008.10.028. URL: http://www.sciencedirect.com/science/article/pii/S0272884208003581.

[57] H. Günzler and H.U. Gremlich. *IR-Spektroskopie: eine Einführung*. German. 4., vollst. überarb. u. aktualisierte Aufl. Weinheim: Wiley-VCH, 2003;2012; ISBN: 3527308016;9783527308019;

[58] E. Pretsch, P. Bühlmann, and M. Badertscher. *Spektroskopische Daten zur Strukturaufklärung organischer Verbindungen*. Berlin, Heidelberg: Springer-Verlag Berlin Heidelberg, 2010. ISBN: 978-3-540-76866-1.

[59] P.H. Howard and W.M. Meylan. *Handbook of physical properties of organic chemicals*. Boca Raton, Fla.: Lewis Publishers, 1997, p. 202. ISBN: 1-56670-227-5.

[60] TU Graz, ed. *Institut für anorganische Chemie: Lab-equipment, Dynamic LS*. 2013. URL: https://www.ac.tugraz.at/index.php/wbPage/wbShow/USER743?lang=en.

[61] Universität Wien, Fakultät für Chemie, ed. *C/H/N elemental analysis: Microanalytical Laboratory*. 2016. URL: https://www.univie.ac.at/Mikrolabor/ind_eng.htm.

[62] B.C. Ranu and S. Banerjee. "Significant rate acceleration of the aza-Michael reaction in water". In: *Tetrahedron Letters* 48.1 (2007), pp. 141–143.

[63] A. Kall, D. Bandyopadhyay, and B.K. Banik. "Microwave-induced aza-Michael reaction in water: a remarkably simple procedure". In: *Synthetic Communications®* 40.12 (2010), pp. 1730–1735.

[64] G. Socrates. *Infrared and Raman characteristic group frequencies: Tables and charts*. 3rd ed. Chichester and New York: Wiley, 2001. ISBN: 0-471-85298-8.

List of Abbreviations

APTES (3-aminopropyl)triethoxysilane

ATR attenuated total reflection

BDODA 1,4-butanediol diacrylate

^{13}C-NMR carbon-13 nuclear magnetic resonance spectroscopy

DLS dynamic light scattering

EPA Environmental Protection Agency

FTIR Fourier transform infrared spectroscopy

GCMS gas chromatography – mass spectroscopy

^{1}H-NMR proton nuclear magnetic resonance spectroscopy

HV hydroxyl value

Jeffamine® D 400 Jeffamine® D polyetheramine (M=430 g/mol)

NMR nuclear magnetic resonance spectroscopy

SiO_2–NP+NH_2 amine-modified silica nanoparticles

PA phthalic anhydride

PEG polyethylene glycol

PPO polypropylene oxide

PTFE polytetraflouroethylene

PTHF polytetrahydrofurane

PTHF250 polytetrahydrofurane (M=250 g/mol)

PTHF250ac polytetrahydrofurane (M=250 g/mol, acrylic terminating groups)

PTHF1000 polytetrahydrofurane (M=1000 g/mol)

PTHF1000ac polytetrahydrofurane (M=1000 g/mol, acrylic terminating groups)

PTHF2000 polytetrahydrofurane (M=2000 g/mol)

PTHF2000ac polytetrahydrofurane (M=2000 g/mol, acrylic terminating groups)

PTHF2900 polytetrahydrofurane (M=2900 g/mol)

PTHF2900ac polytetrahydrofurane (M=2900 g/mol, acrylic terminating groups)

PTMO polytetramethyleneoxide

p-TSA p-toluene sulphonic acid

PUR polyurethane elastomers

pyGCMS pyrolysis gas chromatography-mass spectroscopy

RT room temperature

TDI toluidene diisocyanate

TGA thermogravimetric analysis

TR transmission

$AlCl_3$ aluminium chloride

CaF_2 calcium fluoride

CAN cerium(IV) ammonium nitrate

CO_2 carbon dioxide

H_2O water

H_3BO_3 boric acid

HCl hydrochloric acid

K_2CO_3 potassium carbonate

KOH potassium hydroxide

Na_2SO_4 sodium sulphate

NaCl sodium chloride

NaOH sodium hydroxide

$SiCl_4$ silicon tetrachloride

SiH_4 silan

SiO_2 silicon dioxide

$Si(OH)_4$ silicic acid

c molar concentration

δ chemical shift

δ_{ref} result of ChemDraw simulation of the chemical shift

E energy of an electromagnetic wave

f functionality

h Planck's constant

H integral value of ^{1}H-NMR peak at the specified chemical shift

H_{th} theoretical number of specified hydrogen atoms per molecule

λ wavelength

m mass

M molar mass

n number of repeating units

ν frequency of an electromagnetic wave

$\tilde{\nu}$ wave number

P_{max} maximum power

t time

g gram

°C degree centigrade

K Kelvin

m^2 square metre

mg milligram

min minute

ml millilitre

nm nanometre

ppm parts per million

s second

W Watt

List of Figures

List of Tables